Self-crosslinked fibrous collagen/chitosan blends: Processing, properties evaluation and monitoring of degradation by bi-fluorescence imaging

P.N. Oliveira, A. Montembault, G. Sudre, P. Alcouffe, Lionel Marcon, Hélène Gehan, François Lux, K. Albespy, V. Centis, D. Campos, et al.

Self-crosslinked fibrous collagen/chitosan blends: processing, properties evaluation and monitoring of degradation by bi-fluorescence imaging

P.N. Oliveira[1*], A. Montembault[1], G. Sudre[1], P. Alcouffe[1], L. Marcon[2], H. Gehan[2], F. Lux[2], K. Albespy[3], V. Centis[3], D. Campos[3], S. Roques[4], M. Meulle[4], M. Renard[4], M. Durand[4,5], Q. Denost[4,5], L. Bordenave[4,5], M. Vandamme[5], E. Chereul[5], M. Vandesteene[6], N. Boucard[6], L. David[1]

[1]IMP, CNRS UMR 5223, Univ Claude Bernard Lyon 1, Univ Lyon, 15 bd Latarjet, 69622 Villeurbanne, FR
[2]ILM, CNRS UMR 5306, Univ Claude Bernard Lyon 1, Univ Lyon, 43 bd du 11 Nov 1918, 69622 Villeurbanne FR
[3]Biom'up, 8, allée Irène Joliot Curie, 69800 Saint Priest, France
[4]CIC1401, CHU Bordeaux, Inserm, Univ Bordeaux, 146 rue Léo Saignat, 33000 Bordeaux, FR
[5]BIOTIS Inserm U1026, Univ Bordeaux, Bioingénierie tissulaire, 146 rue Léo Saignat, Bordeaux, 33000, FR
[5]Voxcan, Marcy l'Etoile 69280, FR
[6]MDB Texinov, Saint-Didier-de-la Tour 38110, FR

**paulaoliveiraqmc@gmail.com*

Abstract

Porous collagen/chitosan scaffolds with different Collagen:Chitosan (Coll:Ch) ratios were prepared by freeze-drying followed by self-crosslinking via dehydrothermal treatment (DHT) and characterized as biomaterials for tissue engineering. Cy7 and Cy5.5 fluorochromes were covalently grafted to collagen and chitosan, respectively. Thus, it was possible, using optical fluorescence imaging of the two fluorochromes, to simultaneously track their *in vivo* biodegradation, in a blend scaffold form. The fluorescence signal evolution, due to the bioresorption, corroborated with histological analysis. *In vitro* cytocompatibility of Coll:Ch blend scaffolds were evaluated with standardized tests. In addition, the scaffolds showed a highly interconnected porous structure. Extent of crosslinking was analyzed by convergent analysis using thermogravimetry, Fourier Transform Infrared Spectroscopy and PBS uptake. The variations observed with these techniques indicate strong interactions between collagen and chitosan (covalent and hydrogen bonds) promoted by the DHT. The mechanical properties were characterized to elucidate the impact of the different processing steps in the sample preparation (DHT, neutralization and sterilization by β-irradiation) and showed a robust processing scheme with low impact of Coll:Ch composition ratio.

Keywords: collagen:chitosan scaffolds; dehydrothermal treatment; bi-fluorescence imaging;

1. Introduction

Polymer blending is a classical strategy to combine the original properties of different polymer components or develop new materials with synergistic properties. Such properties may result from

intermacromolecular interactions which in turn impact the macromolecular mobility and the microstructure at different scales [1, 2]. Natural polymer blends are widely envisioned for biomedical applications due to the biological properties of their individual components. They also exhibit several specific advantages, such as their availability from renewable sources, or the easiness of chemical modifications to adapt their properties [3, 4]. Collagen and chitosan are widely used or studied as biomaterials [1, 5]. Their complementary properties may be exploited to design biopolymer blends with finely tuned properties. Both biopolymers are non-cytotoxic, biodegradable, weakly antigenic in comparison with other proteins such as albumin [3, 4] or other polysaccharides such as alginates or cellulose [6].

Collagens have been found in applications as scaffolds in tissue engineering and regenerative medicine [7-9]. Collagens of different types are commonly found in bone, skin, tendon, cartilage and other connective tissues. Structurally, type I collagen is comprised of left-handed, three parallel polypeptide chains coiled around each other to form a right-handed triple helix conformation [10]. These tropocollagen trimers hierarchically associate to form nanofibrils and microfibrils. Collagen contains acidic and basic amino acid residues, such as glycine, proline, hydroxyproline and lysine; it may be either positively or negatively charged depending on the environmental conditions (pH). Collagen can be easily modified, crosslinked and can be blended/associated with other polymers, such as cellulose, fucoidan, poly(l-lactide-co-ε-caprolactone) and poly(3-hydroxybutyrate-co-3-hydroxyvalerate), in a variety of physical forms like fibers, films and nanofibrous scaffolds [8, 9, 11, 12]. Chitosans constitute a family of linear copolymers of D-glucosamine and *N*-acetyl-D-glucosamine with β (1→4) glycosidic linkages. They are usually prepared by *N*-deacetylation of chitin under alkaline conditions [13]. The molar fraction of *N*-acetylated units, *i.e.* the degree of *N*-acetylation (DA), is a structural parameter impacting charge density, hydrophilicity, solubility in aqueous acidic media [14] and crystallinity in the neutralized state [15]. Chitosans with higher DA exhibit faster biodegradation rates partly due to enzymatic degradation [16, 17]. Additionally, chitosan has both reactive amino and hydroxyl groups that can be used for crosslinking and/or chemical modifications [18].

Collagen and chitosan have already been blended in a variety of biocomposites or biomaterials, including porous matrices. They have been developed for various biomedical purposes, such as controlled

delivery of therapeutic agents, skin regeneration, bone tissue engineering and cell culture [19-22]. It is well known that untreated collagen presents a fast biodegradation rate and low mechanical strength, which are the main limitations for the use of this material. However, it was previously evidenced that the addition of chitosan significantly interacts with the nanofibrillar structure of collagen, leading to a reinforcement of the fibrillary network by crosslinking (physical or covalent) and an increases of the pore size of the scaffolds (in the freeze dried form) [4, 23-25]. Collagen/chitosan physical interactions are due to electrostatic interactions and hydrogen bonding [17, 26]. In addition to the physical blend preparation, self-crosslinking the blend is an effective method to modify the biodegradation rate and to optimize the mechanical properties. This process can be performed by a dehydrothermal treatment (DHT) that allows preserving the biocompatibility of collagen and chitosan without adding any cytotoxic crosslinkers [27]. DHT is a physical treatment that consists in heating collagen above 90 °C under vacuum to promote water desorption. This process results in the formation of crosslinks through a condensation reaction between amino and carboxyl groups, yielding amide bonds. It can also occur by esterification through the reaction between carbonyl and hydroxyl groups. These reactions can occur internally in collagen and/or between collagen and chitosan in the case of blends [28, 29].

In the development of *in vivo* resorbable biomaterials, the evaluation of the inflammatory response and of the biodegradation is of primary importance. The resorption kinetics should ideally correspond to the reconstruction of a new tissue in place of the implant. If the degradation is too fast, the support for tissue growth will not be efficient, whereas a too slow degradation can result in fibrosis [26, 30, 31]. Inflammation, biodegradation and tissue reconstruction are classically studied by various histological methods. However, they may require large animal cohorts to obtain a longitudinal following and statistical significance. Recently, advances in biomedical imaging have permitted *in vivo* tracking of material over time in a non-invasive manner, with the combined use of imaging technics, such as Magnetic Resonance Imaging (MRI) [32], X-ray computed tomography (CT) [33] and fluorescence imaging [34]. Such tools cast new light on the biomaterials degradation and their interactions with surrounding cells and tissues; they also give precious information regarding the biodistribution of degraded products. Fluorescence imaging presents great

advantages in small animal studies**:** it enables high sensitivity, non-invasiveness (it is a non-ionizing technique), long-term observations and semi-quantitative measurements [35-38]. To this aim, fluorescent probe molecules (*e.g.*, fluorescein or protoporphyrin) need to be covalently immobilized in biomaterials [34, 39, 40]. The impact of such chemical modification needs to be evaluated even if a small quantity of fluorophores is grafted. Ma *et al.* prepared porous materials using both collagen and chitosan, labelled with rhodamine and crosslinked with glutaraldehyde to observe the infiltration and proliferation of human fibroblasts *in vitro*. They simultaneously observed by fluorescence the distribution of collagen:chitosan blend using rhodamine labelled collagen and fluorescein labelled chitosan. They could observe the infiltration of fibroblasts and characterize the distribution of collagen and chitosan in the scaffold [4]. The simultaneous observation of biodegradation of different collagen:chitosan blends *in vivo* using fluorescence imaging can yield precious informations of collagen and chitosan behaviors during the resorption process. In this work, we prepared collagen:chitosan blends using covalently labelled polymers with different fluorochromes, namely N-hydroxysuccinimide (NHS) modified cyanines Cy7-NHS ($\lambda_{exc}/\lambda_{em}$ 747/800 nm) and Cy5.5-NHS ($\lambda_{exc}/\lambda_{em}$ 675/720 nm) for collagen and chitosan, respectively. These fluorochromes are suitable for *in vivo* near-infrared (NIR) imaging experiments and are able to label amino groups in biomaterials. The degradation of the material can be tracked through the calculation of fluorescence intensity *in situ* and can be used to optimize the material blending and self-crosslinking [34].

The aim of the present work is to study the effect of composition and self-crosslinking method (DHT) on the key biomaterial properties, comprising the *in vivo* resorption of scaffolds obtained with different collagen:chitosan (Coll:Ch) composition ratios, in a final freeze dried form. Three compositions, namely Coll:Ch at the ratio 3:1, 2:1 and 1:1 (w/w) and two chitosans with different DAs, Ch80 (DA ≅ 16 %) and Ch95 (DA ≅ 3 %) were selected. Consequently, a range of physico-chemical and biological behaviors were obtained and characterized: micronrange porous morphology, thermal degradation, swelling, mechanical properties, cytocompatibility and *in vivo* biodegradation rate, using non-invasive fluorescence imaging. To strengthen the interest of labelled materials for the estimation of biodegradation rates, we verified that fluorescent labelling had no impact on the physicochemical and biological behaviors of the

collagen:chitosan blends. Therefore, labelled and unlabelled materials were studied *in vivo* (mouse model) and compared by means of histological analyses.

2. Materials and methods

2.1. Materials

Fibrous collagen from pig tendons (type I collagen) was supplied by Biom'up (St. Priest, FR) and it was extracted in acidic conditions. In brief, tendons were cut into small pieces and processed with several acetone baths for fat removal. Subsequently, the tendons were processed with several baths in hydrochloric acid (HCl) in order to solubilize the collagen fibers. After, a viral inactivation was performed in 1 M NaOH as per World Health Organization requirements. Then, collagen fibers were precipitated in NaCl saline solution and air dried. GMP chitosans were bought, from Heppe Medical Gmbh as Heppe 80/100 (Ch80) and Heppe 95/100 (Ch95), produced from snow crabs (*Chinoecetes opilio*). Cy5.5-NHS ester (M_W 1376 g/mol, $\lambda_{exc}/\lambda_{em}$ 675/694 nm) and Cy7-NHS ester (M_W 818 g/mol, $\lambda_{exc}/\lambda_{em}$ 747/776 nm) were purchased from GE Healthcare and separately dissolved in dimethyl sulfoxide to obtain 1 mg/mL stock solutions.

2.2. Methods

2.2.1. *Chitosan processing and characterization*

2.2.1.1. *Filtration of chitosan*

Chitosans samples, Ch80 and Ch95 were dissolved at 0.5% (w/v) in a stoichiometric amount of aqueous acetic acid (AcOH) and the resulting solutions were successively filtered on membranes (Millipore) of decreasing porosity: 3, 1.2, 0.8 and 0.45 µm. Then, the polymers were precipitated with aqueous ammonia (28%) until pH 9–10. After repeated washings with deionized water (until pH ≅ 6), the neutral precipitates were freeze-dried. This step was performed to remove insoluble particles (impurities) from raw chitosan. Chitosans were then characterized and used in our study.

2.2.1.2. *Characterization of chitosan*

The DA was determined by ^{1}H NMR spectroscopy (Brucker Avance III, 400 MHz) at 25 °C according to the Hirai *et al.* method [41]. The samples were prepared by dissolving 8 mg of chitosan in 1 mL of D_2O and 5 µl of HCl (37 %). The mass average molar mass M_w and the dispersity ($Đ$) were measured by size exclusion

chromatography (2500 and 6000 PW TSK gel columns from Tosohaas) coupled on-line with a differential refractometer (Wyatt Optilab T-rEx) and a multiangle laser light scattering detector (Wyatt Dawn EOS) operating at λ = 633 nm. A degassed 0.2 M acetic acid/0.15 M ammonium acetate buffer with a pH 4.5 was used as eluent. Chitosan acetate buffer solutions at the concentration of 1 mg/mL of chitosan were prepared and analyzed. The flow rate was maintained at 0.5 mL/min. The refractive index increments (d*n*/d*c*) for the two chitosans were determined according to a previous works [42]. The chitosan characterization results are shown in Table 1.

Table 1
Characterization results of the chitosans used in this study:

Samples	DA (%) from NMR	d*n*/d*c* (mL/g)	M_W (g/mol)	M_n (g/mol)	Đ
Ch80	16.3 ± 0.5	0.185	1.58×10^5	9.62×10^4	1.6
Ch95	2.9 ± 0.5	0.196	1.42×10^5	9.76×10^4	1.5

2.2.2. *Synthesis and characterization of labelled chitosan and collagen*

Chitosan (Ch95) was dissolved in AcOH aqueous solution (0.1 M) to reach a concentration of 1 mg/mL. Cy5.5-NHS was then added dropwise and the reaction was left to proceed under magnetic stirring for 12 h at 20°C. The glass bottle was wrapped in an aluminum foil to prevent photodegradation of the dye. 40 mL of NaOH 1 M were subsequently added to precipitate the labelled chitosan. Then, chitosan was split into 50 mL Falcon conical tubes (Corning) and washed 3 times with NaOH 1M by centrifuging the suspension and removing the supernatant. The chitosan precipitate was dialyzed against AcOH 0.1 M (pH around 6-7) to remove unbound dyes by using Vivacell 100 (Sartorius Stedim Biotech, Germany) centrifugal filter device with a molecular weight cut-off (MWCO) of 5 kDa and a polyethersulfone membrane (centrifugation parameters: 2,000 rpm, 20°C). The absorbance of washing water was checked at 675 nm (Varian Cary UV-Vis spectrophotometer 50 scans run by Cary Win UV version 3.00 software) to confirm that all the free dye had been removed from the sample. Then, chitosan was precipitated by addition of NaOH 1 M, washed with deionized water and centrifuged (until pH ≅ 6). Finally, the precipitated chitosan was resuspended in 20 mL deionized water, frozen (12 h) and freeze-dried (48 h).

Collagen was dissolved in AcOH aqueous solution (0.1 M) to reach a concentration of 0.25% w/v. The pH was checked and adjusted to a value around 3 by addition of HCl aqueous solution (0.1 M). Cy7-NHS was then added dropwise and the reaction was left to proceed under magnetic stirring for 12 h at room temperature. The amount of added dye was calculated to functionalize a small amount (about 5 %) of the free amines exposed by collagen (lysine, 3.5 % in mass of collagen). The collagen was protected with aluminum foil to prevent photodegradation of the dye. 11 g of NaCl (final concentration 2 M) were subsequently added to precipitate the labelled collagen. The aqueous suspension was then stirred for 20 min. The sample was then split into 50 mL Falcon conical tubes and centrifuged. The supernatant was discarded and the sample was washed in deionized water and centrifuged. The labelled collagen was then dialyzed against AcOH (0.1 M) (pH around 6-7) using Vivacell 100 (Sartorius Stedim Biotech, Germany) centrifugal filter device with a MWCO of 5 kDa as previously described. Here, the washing water absorbance was checked at 747 nm to confirm that all the free dye had been removed from the sample. Then, the collagen was precipitated again with NaCl and washed with deionized water with intermediary centrifugations (6 times). Finally, the precipitated collagen was resuspended in 30 mL deionized water, frozen (12 h) and freeze-dried (48 h).

The quantification of fluorochrome attached on chitosan and collagen was performed using a Varian Cary UV-Vis spectrophotometer 50 scan run by Cary Win UV version 3.00 software. First, it was verified that neither unmodified chitosan nor unmodified collagen dissolved in AcOH exhibited significant absorption between 600 and 800 nm. To quantify Cy5.5 in modified chitosan (Ch95), reference solutions were prepared by mixing the appropriate volume of Cy5.5 mother solution (1 mg/mL in DMSO) with AcOH 0.1 M aqueous solution to reach cytochrome concentrations ranging from 0 to 0.067 mg/mL and free chitosan in concentration similar to the analyzed sample. Absorbance was measured at 675 nm in triplicate to establish a calibration curve showing absorbance *vs.* concentration. Cy5.5-chitosan sample was characterized by dissolving 13.6 mg chitosan-Cy5.5 in 2 mL AcOH 0.1 M. It exhibited an absorbance of 1.38 corresponding to a Cy5.5 concentration of 8.36×10^{-3} mg/mL (see SM-Fig. 1 (A)), thus a molar ratio of 6142:1, Ch:Cy5.5, corresponding to the grafting of 0.016 % of amino groups of chitosan.

For the quantification of Cy7 covalently bound on collagen the absorbance was measured at 747 nm in triplicate. Again, standard solutions were prepared by mixing the appropriate volume of Cy7 mother solution (1 mg/mL in DMSO) with AcOH aqueous solution (0.1 M) to reach cytochrome concentrations ranging from 0 to 0.053 mg/mL and free collagen in concentration similar to the analyzed sample. Absorbance was measured at 747 nm in triplicate to establish a calibration curve showing absorbance *vs.* concentration. 11.1 mg of collagen-Cy7 were dissolved in 2 mL of AcOH 0.1 M aqueous solution. It exhibited an absorbance of 0.85 corresponding to a Cy7 concentration of 2.38×10^{-2} mg/mL (see SM-Fig. 1(B)), thus a molar ratio of 39.14:1, Lysine:Cy7, respectively. This ratio corresponds to the grafting of 2.55 % of the free amino groups (lysine) of collagen.

2.2.3. *Preparation of freeze-dried samples*

Freeze-dried samples were prepared from the mix of aqueous acidic solutions of collagen (Coll) and chitosan (Ch) using a fixed mass concentration of 1% (w/w) for both solutions. The acid used to solubilize chitosan (pH ≅ 4.5) and to adjust the pH of collagen solution (pH ≅ 3) was HCl. Blend solutions were prepared with various Coll:Ch mass ratios (3:1, 2:1 and 1:1). The solutions were stirred using a conventional magnetic stirrer for 3 h, at room temperature. Then, the solutions were centrifuged (to remove the bubbles). 6 g of solution were then poured in Teflon dishes (diameter of 5 cm), frozen (12 h) and freeze-dried (72 h). Last, the freeze-dried samples were submitted to the DHT, at 120 °C for 24 h under static vacuum (dynamic vacuum was performed during the 1st hour). Subsequently, the samples were neutralized by immersion in PBS solution (pH = 7.3) for 1.5 h and washed with deinized water until pH ≅ 6. Then the washed samples were frozen (12 h) and freeze-dried again (72 h). This protocol was also used to prepare samples with labelled chitosan and collagen alone. Before all biological tests '*in vitro*' and '*in vivo*', the samples were sterilized by β-irradiation (at a dose close to 25 kGy) (IOISOS, Dagneux, France).

2.2.4. *Collagen:chitosan blends characterization*

2.2.4.1. *Scanning electron microscopy*

The microstructure of Coll:Ch, Coll and Ch freeze-dried samples was observed with a field emission gun SEM (FEI Quanta 250). The sections were observed in the low vacuum mode using an acceleration voltage

of 10 kV to avoid charge effects. The surfaces were observed in the high vacuum mode using an acceleration voltage of 2 kV.

2.2.4.2. ***Swelling of samples***

The swelling was measured after immersion of the neutralized samples in phosphate-buffer saline solution (PBS, pH = 7.3). After determined incubation times, starting at 3 min, the samples were gently drained by putting them between two sheets of absorbing paper and weighted. The swelling was deduced from the masses of the sample using the following equation (1):

$$Swelling\ (\%) = \frac{(m - m_0)}{m_0} \times 100 \qquad (1)$$

where m is the mass of the blend after immersion in PBS and m_0 is the mass of the blend before immersion. Samples of 1 cm^2 were studied for each system (n = 4) and the results are an average swelling (%) varying with immersion time.

2.2.4.3. *Thermal characterization*

Thermogravimetric analyses were performed using TA Instruments TGA-Q500 at a heating rate of 10 $°C.min^{-1}$, under inert atmosphere. We also obtained the derivative curves for all analyzed samples. The characteristic temperatures at maximum decomposition rate of the investigated samples were determined. The derivative curves were further processed by the deconvolution using Gauss functions (Origin software, OriginLab Corporation). The peaks were numbered according to increasing temperatures.

2.2.4.4. *FT-IR spectroscopy*

Infrared spectra were recorded on a Thermo Scientific Nicolet iS-10 FTIR spectrometer, equipped with a diamond ATR accessory. In all cases, IR spectra were recorded by accumulation of 200 scans using the ATR accessory, with a resolution of 4 cm^{-1}. The samples were analyzed in their original form of scaffolds, in the case of Coll:Ch blends, and pressed material, in the case of raw chitosans and collagen. For the blends, five spectra were collected at different points to evaluate the homogeneity of the samples and averages of these spectra are used for the analyses shown below.

2.2.4.5. *Mechanical properties*

The tensile properties of the freeze-dried Coll:Ch blends were investigated by using a Testing Machine (SHIMADZU AgX 10kN). The specimens were cut into rectangular slabs in a size of 4 × 40 mm with a sample effective gauge length of about 20 mm. Four specimens were tested for each group of freeze-dried samples. The loading rate was set as 0.1 mm/s. Force-displacement curves were converted to normalized force/nominal deformation, by dividing the applied force load by the lineic density of the sample (ρ_L = m/L, where m is the mass of sample in g and L the total length in mm). From this nominal stress/strain curve, we determined the apparent elastic modulus (corresponding to the slope of the initial linear portion of the stress-strain curve) and apparent stress at rupture, σ_R *i.e.* the maximum tensile stress before rupture. Nominal deformation at rupture, ε_R, was defined as $\Delta L_R/L_0$, where ΔL_R is the elongation at rupture and L_0 is the initial length.

2.2.4.6. *In vitro cytotoxicity of collagen:chitosan scaffolds*

According to ISO 10993-5 standard, two techniques were used to evaluate the cytotoxicity of released products generated by collagen, chitosans and collagen:chitosan blends: (*i*) evaluating cell viability (neutral red assay (NR) by the rapid uptake of a dye into the lysosomes of viable cells) [43] and (*ii*) quantifying cell metabolic activity (tetrazolium dye MTT test) by formazan crystals generation [44]. Prior to these two tests, American Type Culture Collection (ATCC) mouse fibroblastic cell lines were cultivated following the provider's recommendations. Briefly, cell monolayer was grown to near confluence in flat bottom microtiter plates and then were exposed to test (samples) or control articles indirectly by fluid extracts during at least 24 h (n = 6). The absorbance was read with a spectrophotometer (540 nm). Three independent experiments were repeated. Cell viability and metabolic activity were expressed in percentage of non-treated cells representing the maximum cell viability or metabolic activity (value 100%). The positive (Latex) and negative (PTFE) cytotoxicity controls had validated the reactivity of the tested cells.

2.2.5. *In vivo evaluation of labelled and unlabelled collagen:chitosan scaffolds*

2.2.5.1. *In vivo implantation and fluorescence imaging*

All animal experiments were performed in accordance with national animal care guidelines (EC directive 2010/63/UE, French decree n° 2013–118), this study was submitted to the ethical committee N°18

(Vet-Agro Sup - Ecole Nationale Vétérinaire de Lyon) and to the MESR (Ministère de l'Enseignement Supérieur et de la Recherche) and received a favorable opinion of the ethical committee on 12/15/2015 (project N° 1556V2) and of the MESR on 01/06/2016 (project N° 201511271427576).

The *in vivo* evaluation of Coll, Ch and Coll:Ch scaffolds was performed using 7 weeks old immunocompetent female hairless SKH1-hrhr (Crl:SKH1-hr) mice, purchased from Charles River (France) and acclimated 1 week before experimentation. The use of this hairless mouse strain optimizes the transdermal detection sensitivity of the fluorescence from the sample. Experiments were performed in a Biosafety level 2 animal unit and laboratory (ABSL-2); and animals were housed collectively on sawdust (Toplite-Select Fine, Safe) in standard filtered cages inside a controlled ventilated rack (XJ Mouse rack, Allentown USA) under a 12 h day/night cycle with free access to tap water and food *ad libidum* (A04 diet, Safe). During all the experimentation, mice were monitored at least once a day and all events were recorded.

In this study, 24 SKH1 mice were divided into 4 groups. The first group was implanted with labelled Coll-Cy7, the second with labelled Ch95-Cy5.5, the third group was implanted with unlabelled Coll:Ch95 (1:1) and the last one was implanted with labelled Coll-Cy7:Ch95-Cy.5.5 (1:1). The unlabelled Coll:Ch95 was used as a reference to assess the impact of the fluorochromes bonded on the samples by histological analyses. Each mouse (6 per group) was subcutaneously double implanted. All implants were cut as squares with an area of 0.25 cm^2. They were hydrated in a 0.9 % NaCl solution during 5 min before implantation. During implantation, the animals were anesthetized with a mix of 2 % isoflurane (Aerrane, Baxter, USA) in oxygen and both implantation sites were prepared by application of chlorhexidine followed by a subcutaneous injection of buprenorphin (BUPRECARE 0.3 mg/mL, AXIENCE) at 0.05 mg/kg. A small incision of about 1 cm was performed on the left and the right side in the dorsal midline of the mice followed by a subcutaneous dissection below the *panniculus carnosus* to create a pocket on each side of the midline into which each implant was placed. The skin was closed by running sutures with Prolene 5/0 (at least 2 sutures) and the area was disinfected by application of an antiseptic solution. Post-surgery observations were performed during two days, including wound and animal behavior verifications.

In order to follow the degradation of the samples by transdermal fluorescence imaging, the data acquisitions were performed on samples labelled by the fluorochromes Cy7 and/or Cy5.5 using a Perkin

Elmer IVIS Spectrum optical imaging system at different times post implantation, *i.e.* at D0, D02, D05, D07, D09, D13, D16, D20, D23 and D28. In standard experiments the chosen couples of wavelengths were first 675 nm (excitation) / 720 nm (emission) – specific to Cy5.5 (chitosan labelling) and then, about 3 seconds later, 745 nm (excitation) / 800 nm (emission) – specific to Cy7 (collagen labelling). During the fluorescence imaging experiments, the animals were maintained under anesthesia with a mix of isoflurane and oxygen as a carrier gas, in ventral decubitus position.

The objective of the fluorescence monitoring is to assess the degradation of collagen and chitosan during 28 days. The expected result is a decrease of the fluorescence signal linked to the degradation of the considered component. To this end, fluorescence intensity quantification was performed in a region of interest (ROI) which was delineated around the implantation site (see Figure 1), but using the same ROI size and shape for all measurements. The data were recorded using the "Living Image" software version 4.4 (IVIS Imaging Systems) yielding, after calibration, the total radiance efficiency ([photons/s/cm²/sr] / [µW/ cm²]) thus accounting for the incident power density.

The data treatment required to subtract the fluorescence background. It was estimated thanks to the measurement performed on a region of interest (ROI) delimited in a site without fluorescent implant. An averaged background level was calculated and the background level was then subtracted to each fluorescence value. The data were normalized to the fluorescence at D00 (t = 0) following Equation 2:

$$F_{c,n}(t) = \frac{F(t) - F_{bck}}{F(t=0) - F_{bck}} \quad (2)$$

where $F_{c,n}(t)$ is the background-corrected normalized fluorescence, F(t) is the raw fluorescence integrated over the ROI at time t, F_{bck} is the background fluorescence, and F(t = 0) is the raw fluorescence integrated in the ROI at day 0.

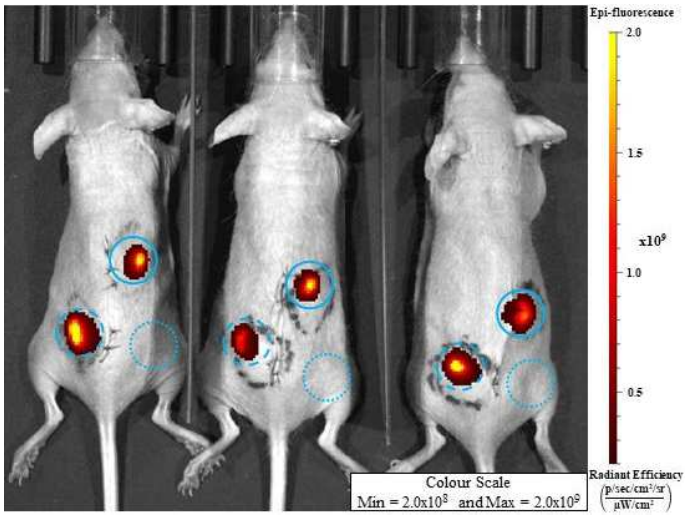

Figure 1 - Example of a fluorescence image obtained with IVIS imaging system. Full circles are ROIs delineated around the right implantation sites. Dashed circles are ROIs delineated around the left implantation sites. Dotted circles are the chosen ROIs for the estimation of the background fluorescence. Tattoos were performed to identify the implantation sites and possible implant migration.

2.2.5.2. Euthanasia and sampling

Animals were euthanized after the last fluorescence acquisition on D07 and D28 by a cervical dislocation under anesthesia (mix of isoflurane and oxygen). At D07, implant sampling was performed on 12 mice and at D28 on the other 12 mice. To this end, mice were anesthetized with isoflurane (1-2%) and oxygen as a carrier gas and then placed in dorsal recumbency. Then implants were surgically removed with skin (the diameter of explanted area was a total at least of 1.5 cm^2). Biopsy tissue was placed in buffered formaldehyde 4% (Q Path®-VWR-FOR0020AF59001) and further processed for histological analyses.

2.2.5.3. Histological analyses

Samples from the explanted collagen (Coll), chitosan (Ch95) and Coll:Ch95 (unlabelled and labelled with their fluorophores) were fixed in 4% formalin, embedded in paraffin and cut into 6-µm sections stained with hemalun-erythrosine-saffran (HES) to evaluate tissue inflammatory reaction and sample resorption.

3. Results and discussion

3.1. Microstructure and physico-chemical characterization of scaffolds

3.1.1. Collagen:chitosan interactions and evaluation of DHT efficacy

The weight loss occurring during thermal degradation of collagen was described to occur in three stages: the first one is assigned to the loss of water (~105 °C); the second one is related to a first thermal

degradation of the polymer chains (320 °C); and the third stage is attributed to the carbonization of the residual polymer material (370 °C) (see SM-Fig. 2) [45]. Chitosans Ch80 and Ch95 present the first maximum of weight loss at 110 °C which is due to evaporation of water loosely bound to the polymer; the thermal degradation events occurring in the range 200-300 °C are attributed to further dehydration, deacetylation and depolymerization of chitosan; the subsequent weight loss, above 300 °C, corresponds to the residual decomposition reactions (see SM-Fig. 2) [46, 47].

The Coll:Ch blends were analyzed before and after the application of DHT to evaluate the crosslinking effect on the thermal behavior of the samples. The thermograms and derivative curves are shown in Figure 2 (A) and (B), respectively, for the Coll:Ch95 blends without treatment, at the ratios 3:1,2:1 and 1:1. The TGA curves result from the presence of collagen and chitosan: the degradation event at lower temperature (~240 °C) corresponds to the degradation of chitosan and the ones located in the higher temperature range (320 -370 °C) to the degradation of collagen. The residual masses were 18.6, 20.8 and 23.3 %, corresponding to the ratio Coll:Ch95, 3:1, 2:1 and 1:1, respectively. The degradation processes are complex, but the deconvolution of the derivatives curves was satisfactory with the presence of 4 peaks that can be attributed to the degradations of collagen and chitosan (Fig 2 (B)). In particular, an increase of the chitosan degradation temperature (I) could be detected, in which the first weight loss shifted from 230 °C (pure chitosan) to 247 °C (in Coll:Ch blend). Another degradation process (II) in Ch95 was shifted from 250 °C to 284 °C. The two other peaks (namely III and IV) are due to the degradation of collagen: (III) remained the same in the blend and in the pure collagen at 320 °C while process (IV) decreased from 370 °C to 355 °C. Such changes in the degradation temperature of collagen and chitosan within the blends can be attributed to interactions between the polymers. However, a real change in the polymer degradation mechanisms could not be evidenced. Accordingly, it was possible to see an evolution in the peak intensities with composition in the blends (see Fig. 2 (B)).

Figure 2 (C) and (D) show the thermograms and their derivative curves for Coll:Ch95 blends, for the ratios 3:1, 2:1, 1:1, that underwent the DHT. The residual masses increased after the DHT and varied with the composition ratio, from 29.9 to 31.6 and 33.7 %, corresponding to the Coll:Ch95 ratios, 3:1, 2:1 and 1:1, respectively. These increases in residual mass values suggest a change in the degradation mechanism after

the DHT. The deconvolutions of the derivative curves show three main degradations between 160 °C and 500 °C (Fig 2 (D)). The degradation profile of Coll:Ch95 blends changed probably due to the DHT that induced the formation of covalent bonds (amide) between collagen and chitosan. The first degradation maximum (I') may be attributed to the degradation of Ch95. A decrease of this degradation temperature was observed with the increase of Ch95 content in the blends, from 292.6 to 288.8 and 268.8 °C, for Coll:Ch95 ratios, 3:1, 2:1 and 1:1, respectively. The second and third degradation maximums (III and IV) can be correlated predominantly to the collagen degradation. These two temperatures decrease with decreasing of collagen content in the blends, from 320 (III) and 370 °C (IV) to 310 and 360 °C. These results can be attributed to the high degree of interactions between collagen and chitosan after the DHT.

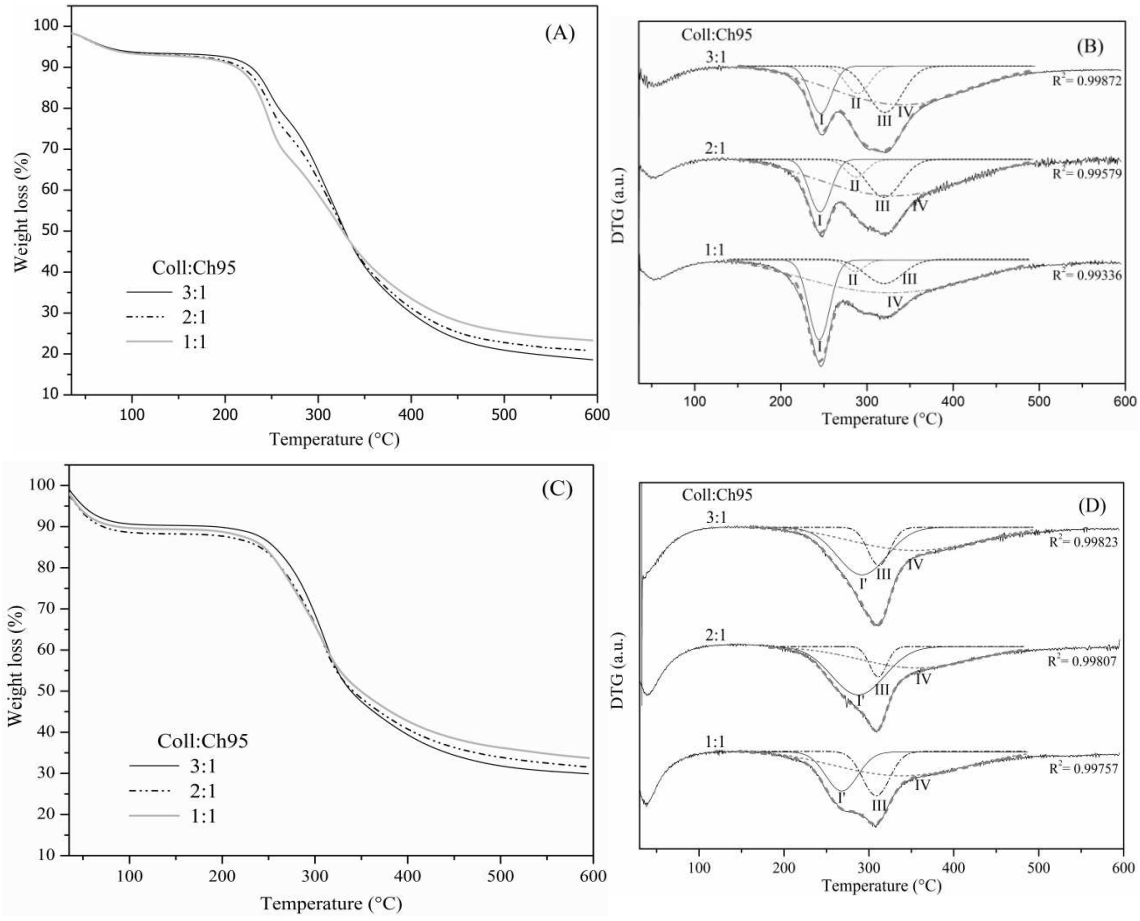

Figure 2 – TGA analysis and derivative curves of the Coll:Ch95 samples without treatment (A) and (B) and after the DHT (C) and (D). The derivative curves were analyzed by OriginLab software and the deconvolution of these curves are shown in (C) and (D).

The TGA analysis was able to detect that the DHT induces strong interactions (covalent bonds) between collagen and chitosan. Others analysis will be described below to quantify and observe the new

behaviors of the samples after the DHT. The same thermal behavior was observed for the Coll:Ch80 samples series (see supporting material, SM-Fig 3).

FTIR spectra of the collagen (fibrous lyophilizate), chitosans (powders) (Ch80 and Ch95 raw material) and the Coll:Ch blends are shown in Figure 3, for different ratios (3B and 3D) and preparation steps (3A and 3C): uncross-linked (without treatment), cross-linked (XL, *i.e.* after DHT) and neutralized (Neu) samples (see section '*Preparation of freeze-dried samples*' above and SM-Table 1 in the Supporting Material, which gives the characteristics absorption bands of collagen and chitosan). FTIR spectra of chitosans (Ch80 and Ch95) present some differences in the range 1680-1480 cm^{-1} due to different DA. In this range, characteristic absorption bands related to the carbonyl group (C=O) of the secondary amide group (1641 cm^{-1}) and the absorption band of the primary amino group -NH_2 (1590 cm^{-1}) can be observed. As expected, the absorption band of the amino group at 1590 cm^{-1} is more intense for Ch95 (DA ≅ 3 %) than for Ch80 (DA ≅ 16 %) (see Figure 3A and 3C) [48, 49]. The main characteristic absorption bands of collagen are present at 1653, 1538 and 1240 cm^{-1} from amide I, II and III. The absorption band at 1653 cm^{-1} for amide I arises from C=O stretching vibrations and amide II absorption band at 1538 cm^{-1} is generally a combination of N-H bending and C-N stretching vibrations. In addition, the absorption band located at 1240 cm^{-1} is attributed to amide III absorption band for C-N stretching and N-H in-plane bending from amide linkages [50, 51]. Additionally, other absorption bands were observed such as the CH_2 asymmetric bending at 1450 cm^{-1} which is a useful internal reference, since its wavenumber and intensity have been reported to be invariant with denaturation and harsh dehydration [52, 53]. Accordingly, in spite of the different processing conditions screened in this study, no significant change in the intensity or shift for this absorption band was observed.

In the Coll:Ch blends (Ch80 or Ch95), the spectra are characterized by the presence of the absorption bands of the pure components, with intensities approximately proportional to the mass fraction of each component, as can be observed in Figure 3B and 3D. It is possible to identify the presence of collagen due to the strong absorptions bands at 1653 and 1538 cm^{-1}, while the absorption bands that are specific to chitosan are located at 1085 and 1029 cm^{-1}. Despite the characteristic identification of collagen and chitosan in the spectra of the blends, the detailed interpretation of the obtained results is difficult because of the complexity

of their chemical structures and the overlapping of their characteristic absorption bands. The spectra of blends are not a simple superposition of the spectra of the separated components due to the presence of interactions between the two polymers by the formation inter and intra-macromolecular hydrogen bonds (before the DHT) and also the formation of covalent bonds resulting from crosslinking (after the DHT). In Figure 3, the absorptions bands centered at 3330 (O-H and N-H stretching) and at 1653 cm^{-1} (amide I, C=O stretching) shift to 3295 and 1638 cm^{-1}, this shift can be considered as a spectroscopic signature of collagen-chitosan interactions. The shifts of the absorption band at 1538 cm^{-1}, corresponding to amide II, N-H bending and C-N stretching vibrations, are as significant as for amide I. The shifts in the absorption bands listed above occurred for both blends, Coll:Ch80 and Coll:Ch95, and their shifts values are similar for the different Coll:Ch ratios.

In addition to the shifts in the absorption bands, the evolution of their intensities can be observed. In the range 3500-3200 cm^{-1}, the decrease of the intensity of the absorption bands between the separated components and the blends could be due to a lower content of free H_2O, as well as, amino and hydroxyl groups due to crosslinking. The absorption band at 1538 cm^{-1} (amide II) is expected to be proportional to the amount of $–NH_2$ in collagen. In the blend, it is proportional to the amino groups of both collagen and chitosan. The DHT induces the formation of amide linkages and consequently induces a decrease in the intensity of absorption band of amide II. In order to characterize amide group formation, we investigated the relative intensity ratio ($r = I_{1538}/I_{1450}$) of the absorption bands at 1538 and 1450 cm^{-1} (invariant) [29, 54]. Since we did not find evidence of ester bond formation (from the absence of absorption bands above 1690 cm^{-1}), it can be concluded that the DHT induced only the formation of amide bonds. Table 2 displays the evolution of values of *r*. The extent of crosslinking was calculated from the relative decrease of this ratio (the sample without treatment was assumed as 0 % of crosslinking). The extent of crosslinking was between 6 and 9 % in the Coll:Ch blends after the DHT. The freeze-dried collagen sample presented the percentage of 16.55 %. Such crosslinking helps to improve the mechanical properties of the blends and limits the swelling of the scaffolds in the freeze-dried form.

The ratio between the relative intensity of collagen amide III absorption band, at 1240 cm^{-1}, and the intensity of the absorption band at 1450 cm^{-1}, $r' = I_{1240}/I_{1450}$, has been used to indicate if the triple-helical

structure of collagen was preserved after the sample preparation [50, 55]. Plepis *et al.* described that a relative intensity of these absorptions bands close to 1.0 is indicative of a preserved collagen triple-helix structure. Such ratio was used for the characterization of gelatin, exhibiting a ratio of 0.59 in the same processing conditions [50]. The values of *r'* are shown in Table 2. They indicate that the collagen triple helix structure was maintained (*r'*~1.0) after the blend formation and the sample treatments (DHT and neutralization).

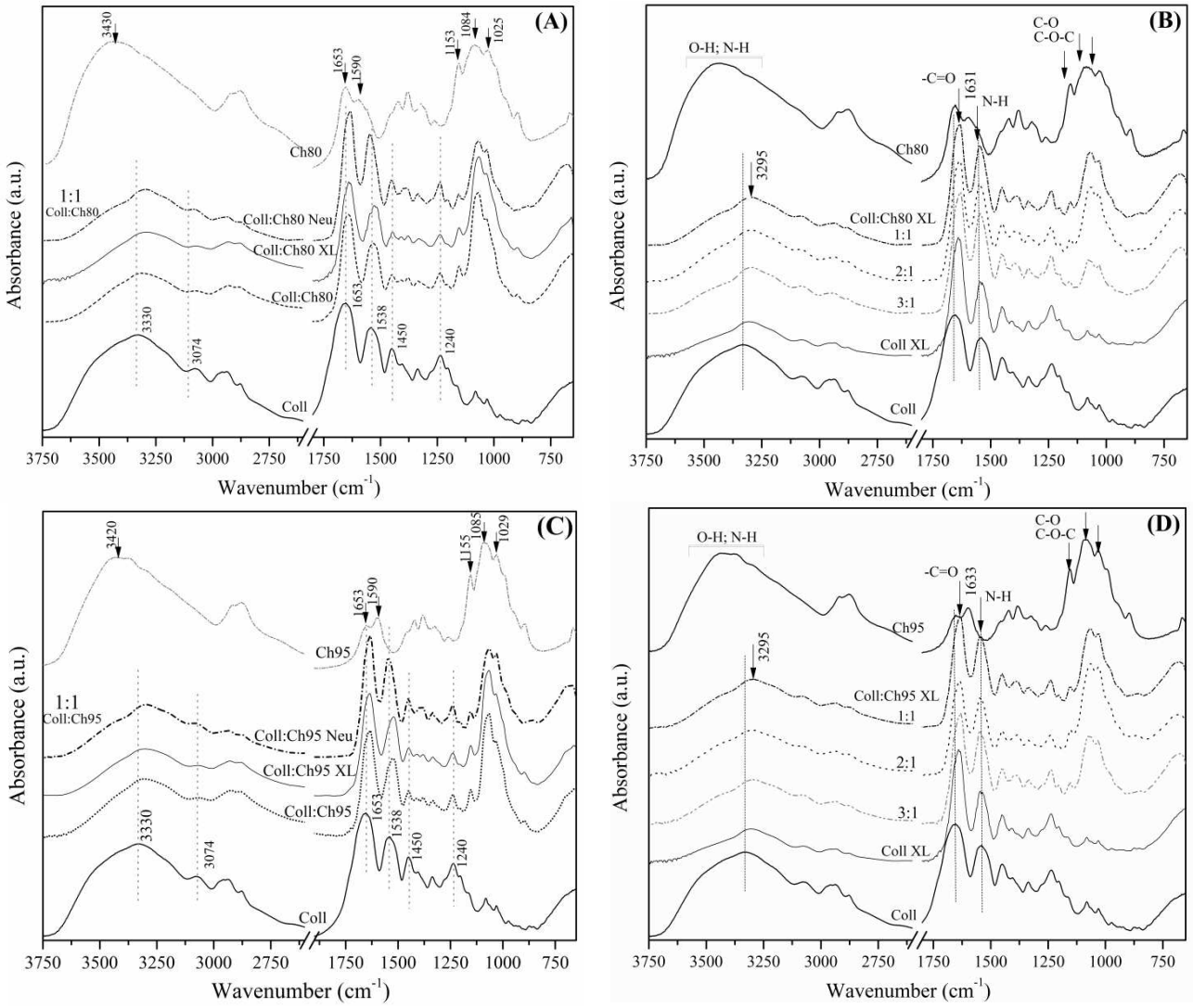

Figure 3 – A - FTIR spectra of Coll, Ch80 and the blend Coll:Ch80 at ratio 1:1 submitted to crosslinking - DHT (XL) and neutralization (Neu) processes; **B** - FTIR spectra of Coll, Coll XL, Ch80 and the blend Coll:Ch80 XL at the ratios 1:1, 2:1 and 3:1; **C** - FTIR spectra of Coll, Ch95 and the blend Col:Ch95 at ratio 1:1 crosslinking - DHT (XL) and neutralization (Neu) processes; **D** - FTIR spectra of Coll, Coll XL, Ch95 and the blend Coll:Ch95 XL at the ratios 1:1, 2:1 and 3:1. (See detailed table with absorption bands of Coll and Ch at the SM-Table 1).

Table 2

Estimation of the extent of crosslinking by the ratio I_{1538}/I_{1455} (r) and verification of the preservation of collagen triple helix structure by the ratio I_{1240}/I_{1450} (r') in collagen and Coll:Ch samples:

Samples	Ratio between the intensities of the absorptions band at 1538 and 1450 cm^{-1} and estimation of the crosslinking efficiency					Ratio between the intensities of the absorptions band at 1240 and 1450 cm^{-1}		
	r		crosslinking[x] (%) in XL samples	r	crosslinking[x] (%) in Neu samples	r'		
	Without treat.	After DHT (XL)		Neu		Without treat.	After DHT XL	Neu
Coll(fiber)	1.27	-	-	-	-	0.89	-	-
Coll *	1.45	1.21	16.55	1.22	15.86	1.00	1.01	0.98
Coll:Ch80 3:1	1.30	1.19	8.46	1.24	4.94	1.01	0.99	0.99
Coll:Ch80 2:1	1.25	1.17	6.40	1.19	4.95	1.01	1.00	0.98
Coll:Ch80 1:1	1.23	1.16	6.66	1.17	5.03	1.00	0.99	0.98
Coll:Ch95 3:1	1.25	1.16	7.20	1.15	7.38	1.00	0.99	0.99
Coll:Ch95 2:1	1.27	1.20	5.51	1.17	8.19	0.98	0.98	0.98
Coll:Ch95 1:1	1.30	1.20	7.69	1.17	11.21	0.98	0.97	0.97

*Coll – collagen freeze-dried sample

[x]extent of crosslinking = $(r|_{\text{whithout DHT}} - r|_{\text{after DHT}})/\ r|_{\text{whithout DHT}}$

3.1.2. Morphology of freeze-dried scaffolds

The microstructure of porous freeze-dried scaffolds potentially has a direct influence on cell migration, attachment, proliferation and function [4, 56]. The cross-sections of the freeze-dried samples are shown in Figure 4. They reveal the classical interconnected porous structure of samples obtained after the freeze-drying process, resulting from the formation of ice crystals constraining the polymer in intercrystalline spaces to form pore walls. The collagen/chitosan blends resulted in a more homogeneous porous structure with a narrower size distribution of the pores in comparison with the freeze-dried pure collagen sample. The pore size was estimated in the direction perpendicular to the plane of the membranes. In the collagen samples, the distribution of pore size is bimodal, with average sizes close to 300 µm and 75 µm. In the Coll:Ch blends, the average pore sizes are ranging between 115 and 200 µm, as reported in Table 3. The neutralization process (*i.e.* swelling in PBS during 1.5 h, washing and freeze-drying) caused an overall decrease in the thickness as can be observed in Figure 4 and Table 3. The initial sample thicknesses were ranging between 2.0 and 2.5 mm; after the neutralization process, this value was reduced three-fold (see Table 3). The pore sizes (in the direction perpendicular to the membrane plane) also decreased after the neutralization process and the variation of the aspect ratio of the pores is directly linked to the thickness evolution ratio (see Table 3 and Figure 4). In spite of the thickness decrease and the evolution of the pore aspect ratio, a significant porous structure was maintained at supra-cellular scale, suggesting the suitability of this biomaterial structure for biomedical applications, such as: suturable material for wound healing,

exudates absorption, hemostasis, adherence prevention, matrices for cell colonization and proliferation and tissue reconstruction. The SEM images of external surfaces display a fibrous material morphology, with collagen fibrils oriented in the plane of the membrane (see Figure 4 –C, K, P, T). This fibrous morphology is also apparent in the pore walls, especially at high collagen content.

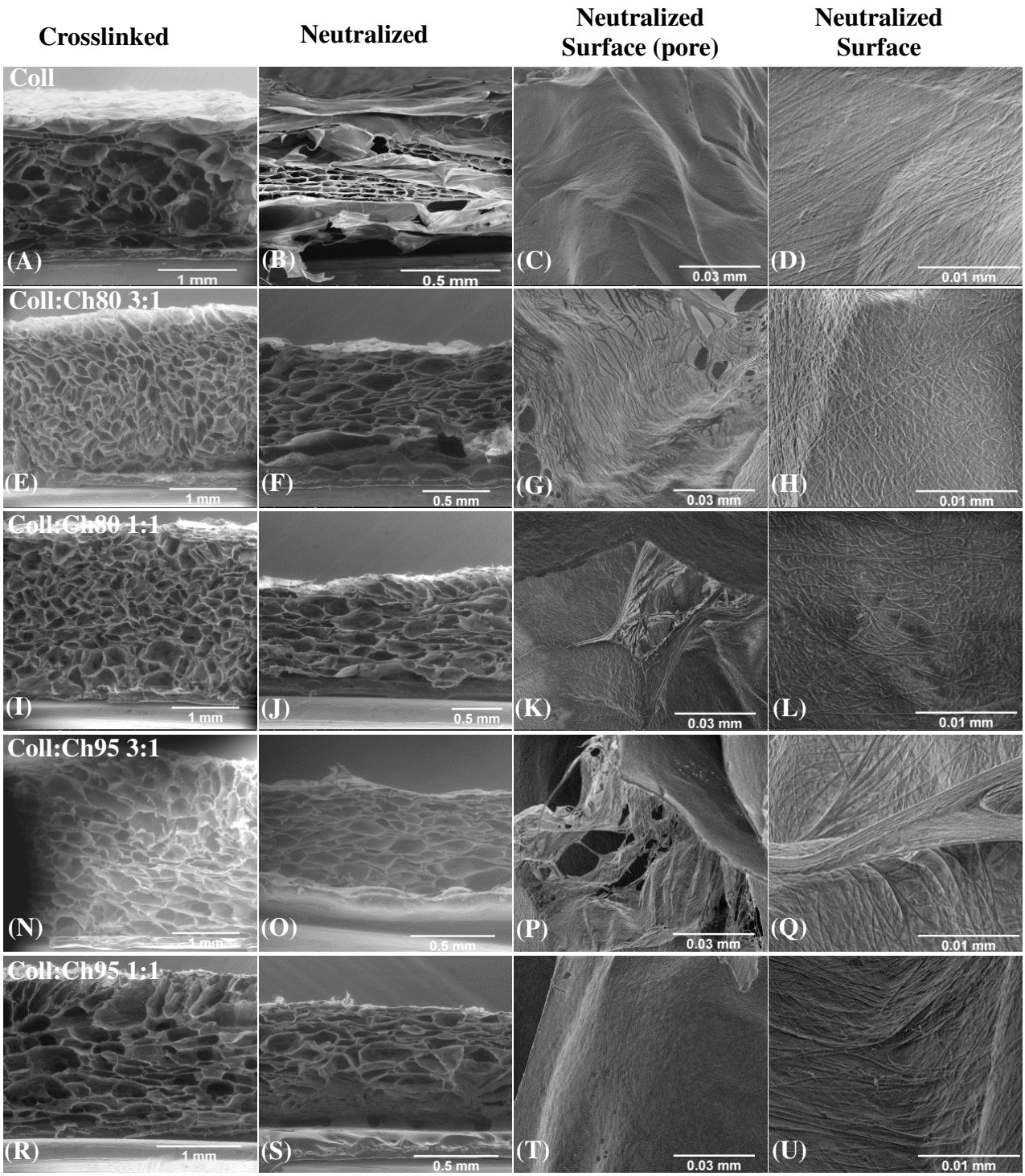

Figure 4 – SEM images of the samples after the DHT (crosslinked) and neutralization process: Coll (A, B, C, and D), Coll:Ch80 3:1 (E, F, G and H), Coll:Ch80 1:1 (I, J, K and L), Coll:Ch95 3:1 (N, O, P and Q) and Coll:Ch95 1:1 (R, S, T and U).

Table 3

Thickness and pore size of samples after the DHT and neutralization process:

Samples	Thickness (mm)	Thickness ratio (XL/Neu)	Pore size (μm)	Pore size ratio (XL/Neu)
Coll XL	2.04±0.04	2.75	300.34±89.02/75.00±20.51*	2.22*
Coll Neu	0.74±0.06		33.75±7.51*	
Coll:Ch80 3:1 XL	2.33±0.07	2.61	207.02±55.40	2.51
Coll:Ch80 3:1 Neu	0.89±0.02		82.41±27.43	
Coll:Ch80 2:1 XL	2.94±0.07	3.19	149.88±50.61	1.29
Coll:Ch80 2:1 Neu	0.92±0.22		116.60±40.00	
Coll:Ch80 1:1 XL	2.52±0.02	2.49	154.94±41.42	1.14
Coll:Ch80 1:1 Neu	1.01±0.10		135.71±42.14	
Coll:Ch95 3:1 XL	2.75±0.13	4.75	169.42±56.86	2.47
Coll:Ch95 3:1 Neu	0.58±0.02		68.70±15.59	
Coll:Ch95 2:1 XL	1.86±0.10	2.86	121.55±34.91	1.284
Coll:Ch95 2:1 Neu	0.65±0.07		94.69±36.78	
Coll:Ch95 1:1 XL	1.91±0.05	2.98	190.82±71.38	2.82
Coll:Ch95 1:1 Neu	0.64±0.03		67.58±30.36	

*Bimodal pore distribution in Coll XL sample. In Coll Neu samples only the small pores were studied, the larger pores collapsed see Figure 3B. The relative evolution of the pore size was calculated using the size evolution of the small pores, perpendicular to the plane of the membrane.

3.1.3. Swelling of samples after the crosslinking process

Rehydration of freeze-dried collagen scaffolds are often required intraoperatively to soften the material, prevent tissue dehydration by material contact and to favor cellular integration. Before the DHT, the Coll:Ch blend samples were not stable in the rehydration solution, thus crosslinking was required. After DHT (120 °C for 24 h under static vacuum), the samples became stable in aqueous medium and could be neutralized. Finally, freeze-dried scaffolds were then submitted to the PBS uptake test, consisting in PBS immersion for at least 3 days, the results are shown in Figure 5. The scaffolds reached the maximum of PBS absorption after approximately 2-3 h of immersion; 75 % of the total mass uptake occurred after 3 min, which is compatible with surgical practice. The plateau uptake increased with the collagen content. Nevertheless, Coll sample exhibited an uptake similar to the one of the blends, and the behavior of blends could not be fully explained invoking a higher hydrophilicity of collagen *vs* chitosan. In both Coll:Ch80 and Coll:Ch95 systems, the rate of absorption after 3 min was higher for the samples with higher porous faction (*i.e.* higher apparent thickness). Thus, as the pore size increased, the PBS solution was absorbed faster. As result, Coll:Ch blends showed a PBS uptake closely related to their porous structure and also their extent of crosslinking. For example, Coll:Ch95 1:1 sample, which presents relatively closed structure and a higher extent of crosslinking, absorbed significantly less PBS than the other systems. The results for blends

processed with Ch80 showed similar uptake levels, in relation with the extents of crosslinking that were very close. Ch95 being more hydrophobic than Ch80 in the neutralized state [15], the different hydrophilicity of the two studied chitosans had a secondary influence on the PBS uptake results: 1:1 blends richer in chitosan exhibited a more hydrophobic character with Coll:Ch95 1:1 absorbing less PBS than Coll:Ch80 1:1.

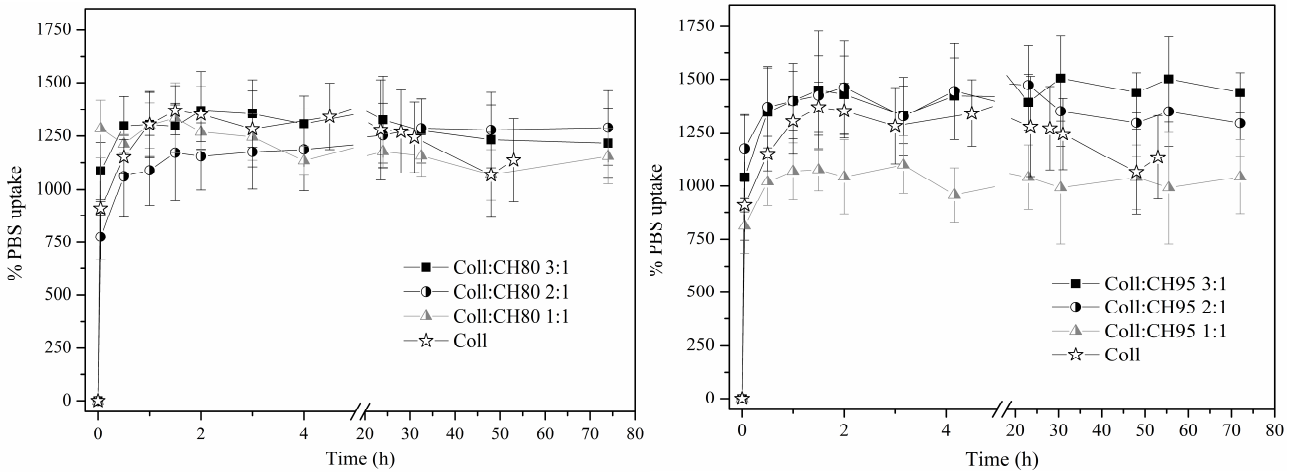

Figure 5 – PBS uptake (% w/w) of samples submitted to crosslinking (DHT) and neutralization processes.

3.1.4. Investigation of the mechanical properties

The application as scaffolds requires mechanical properties according to specific tissue and implantation site, as well as to specific surgical procedures. The effect of the fabrication process on the mechanical properties of the Coll, Ch and Coll:Ch blends (n = 4) was analyzed at different steps of their processing. Thus, the impact of the sterilization by β-irradiation was also analyzed. We finally investigated the effect of hydration, simulating the real conditions of implantation. Again, in this analysis, pure chitosan hydrochloride freeze-dried samples could not be investigated after neutralization since they are soluble in PBS solution.

The typical stress-strain curve of a selected sample is shown in the supporting material (see SM-Fig. 4). The mechanical behavior (Young's modulus *E*, apparent stress at break σ_R and nominal deformation at break ε_R) of collagen, chitosans (Ch80 and Ch95) and Coll:Ch blends are shown in Figure 6. Figure 6 (A_1) and (B_1) display Young's moduli of samples at different steps of their fabrication process. The impact of composition is clearly evidenced in freeze-dried samples, chitosan acting as a binder for collagen fibrils

(both before and after DHT). However, the values of the modulus of Coll:Ch blends, *Ec*, stay above the Voigt law (upper bound for the prediction of elastic modulus of two-phase composites), as written in Equation 3:

$$Ec \geq \varphi_{Coll} * E_{Coll} + (1 - \varphi_{Coll}) * E_{Ch} \quad \textbf{Eq. 3}$$

where φ_{Coll} is the collagen volume fraction, E_{Coll} and E_{Ch} the individual modulus of collagen and chitosan respectively. This result suggests a synergetic effect originating from the coupling of two components. In addition to form a matrix around collagen fibrils, both Ch80 and Ch95 could play a role in an interfibrillar bonding, thus contributing to a more efficient collagen fibril network. β-irradiation sterilization did not drastically decrease the Young's modulus of blended samples, as shown in Figure $6A_1$ and $6B_1$. As expected, a strong reduction of the Young's moduli was observed after the rehydration process (3 min in PBS). Water acts as a plasticizer for both collagen and chitosan, although the presence of chitosan limited the decrease of the elastic modulus.

The evolution with processing and composition of the apparent stress at rupture (σ_R) is shown in Figure $6A_2$ and $6B_2$. Coll:Ch80 and Coll:Ch95 blends present similar values of σ_R. Pure chitosan samples are the most fragile, and pure collagen exhibits the highest strengths. Here again, the performance of the blends are close or even higher than the prediction of the Voigt model (*i.e.* parallel mechanical coupling for the prediction of rupture stress of a two phase composite). This is indicative of chitosan/collagen interactions, in particular for the crosslinked systems after DHT. The nominal deformation at rupture (ε_R) of freeze-dried, crosslinked and sterilized collagen, chitosans and blend samples (Coll:Ch80 and Coll:Ch95) were similar, as can be observed in Figure $6A_3$ and $6B_3$. After hydration, collagen and Coll:Ch blends kept high ε_R values, as a result of water plasticization. As a general trend, this mechanical analysis validated the processing of the blends, including the sterilization step. The mechanical properties of the blends are favorably impacted by collagen-chitosan interactions, although part of the synergistic properties (*e.g.* observed for Coll:Ch 3:1 blends) are lost after sterilization, possibly due to a degradation of both components and/or their interaction state.

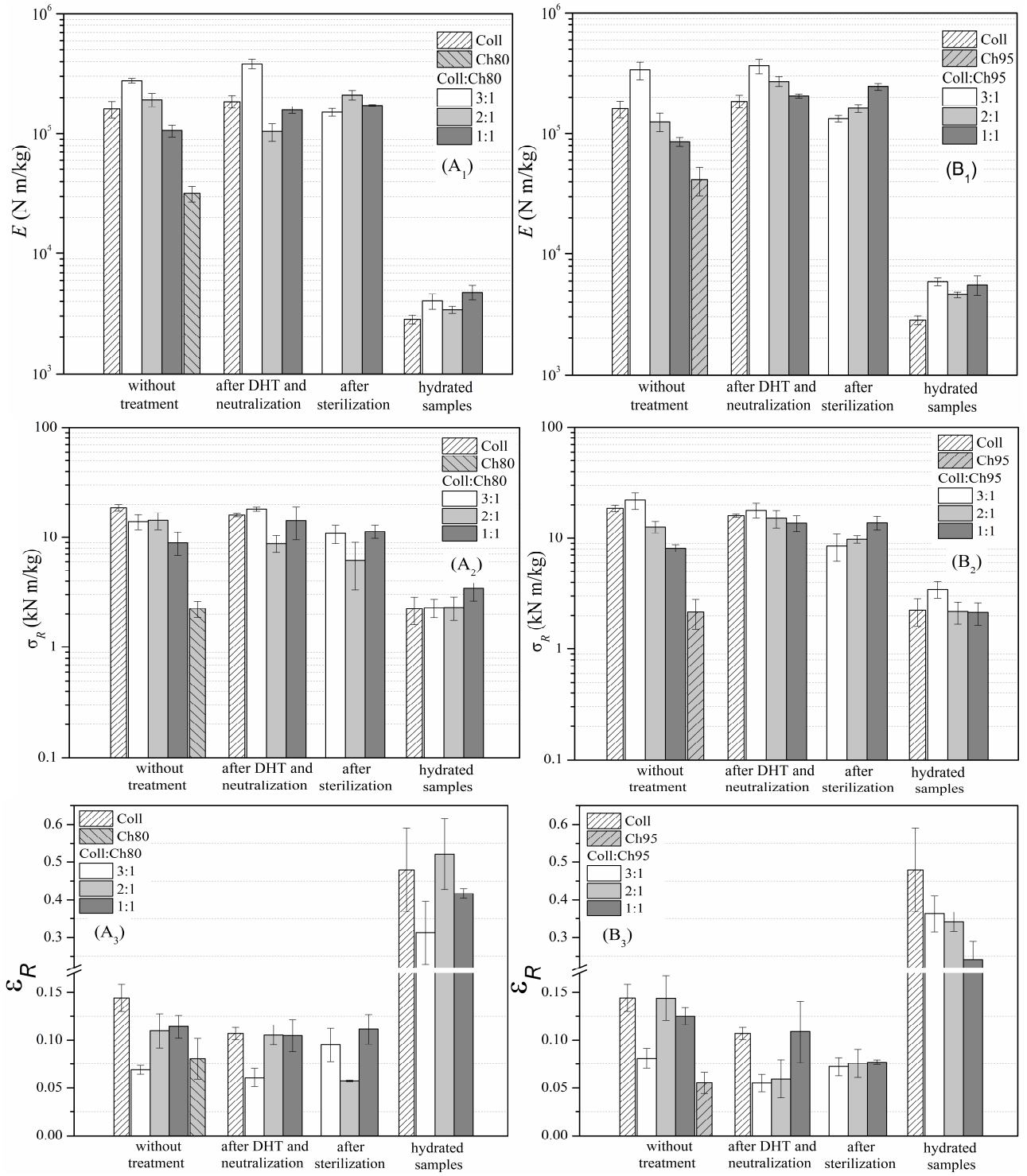

Figure 6 - Mechanical analysis by tensile tests of pure and blended samples, before and after being submitted to different treatments. *E* is the Young's modulus and is shown in A_1 and B_1, σ_R is the apparent stress at rupture and is shown in A_2 and B_2 and ε_R is the nominal deformation at rupture and is shown in A_3 and B_3.

In the first section of this work, the evaluation of the properties of self-crosslinked collagen-chitosan blends validated the preparation process of rehydratable freeze-dried scaffolds exhibiting sufficient

mechanical properties in the hydrated state for intraoperative handling and suturing. In fact, Coll:Ch composition ratio had a modest impact on the final mechanical properties. In the second section, we studied and compared the biological properties (*in vitro* and *in vivo*) of the blends and integrated this comparative evaluation in the choice of the best collagen/chitosan association for the design of a resorbable implant. These biomaterial evaluations consisted in the cytotoxicity determination, the resorption kinetics and histological analyses for the local scale resorption process, cellular infiltration and inflammatory response.

3.2. *In vitro* cytotoxicity

Figure 7 displays cellular viability (7A and 7B) and cellular metabolic activity (7C and 7D) of the final Coll:Ch blends. Regarding the ISO 10993-5 standard, the threshold below which a biomaterial is cytotoxic is 70% (dashed line in Figure 7). The positive and negative controls showed that the assays were validated. For Coll:Ch80 samples, the cell survival was above 70% for the ratios 3:1 and 2:1, but not for the ratio 1:1. On the other hand, the metabolic activity was higher than 70% for all Coll:Ch80 ratios, showing that the cells survived with Coll:Ch80 at the ratio 1:1 and that the extracted vehicles were healthy, as shown in the Figure 7C. For Coll:Ch95, the survival rate was above 70% for all Coll:Ch95 ratios, as shown in the Figure 7 B. However, the metabolic activity of the surviving cells was lower than 70 % (see Figure 7D). We conclude that the cytotoxicity profile of Coll:Ch80 materials was more favorable and the cytotoxicity results of Coll:Ch95 samples were contradictory. Thus, only the metabolic activity seemed to be impacted by the DA of chitosan. The Coll:Ch ratio did not significantly change the cytotoxicity nor the metabolic activity.

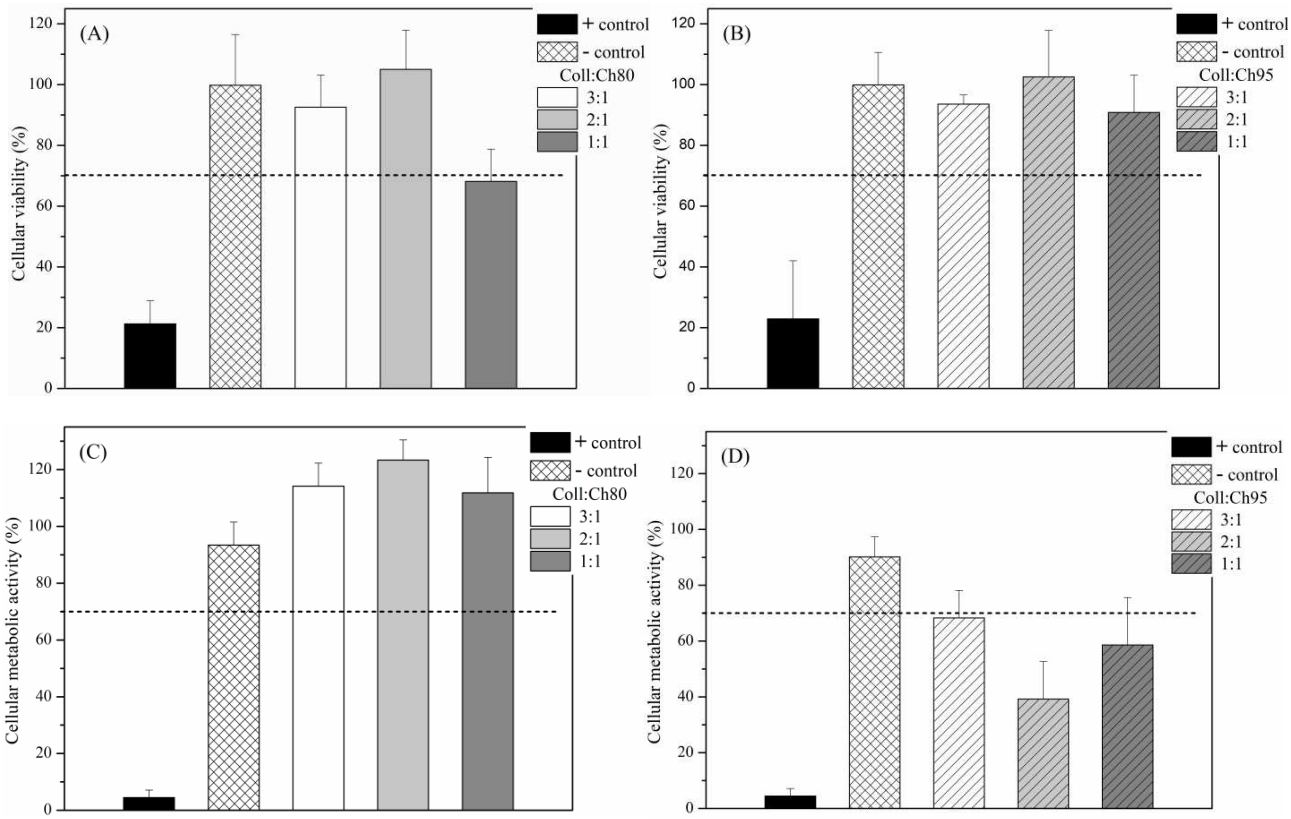

Figure 7 - Extract cytotoxicity of Coll:Ch scaffolds. Cellular viability was assessed by Neutral Red test (NR) (7A and 7B) and cellular metabolic activity assessed by MTT test (7C and 7D) to evaluate the survival and metabolic activity of fibroblast mouse's cell lines, respectively.

3.3. *In vivo* evaluation of resorption of collagen:chitosan scaffolds

3.3.1. Fluorescence imaging and preliminary quantification of scaffold degradation by fluorescence

Before implantation, sample fluorescence was evaluated *in vitro* to verify that the signal would be sufficient to allow an *in vivo* follow-up. The preliminary results can be observed in SM-Fig 5. The fluorescence signals emitted by all the implants (for labelled collagen and chitosan) were much higher than the background level (3.9×10^8 [p/s]/[µW/cm²]). The fluorescence emitted by the Coll-Cy7 sample was, on average, of $4.2 \times 10^9 \pm 2.8 \times 10^8$ [p/s]/[µW/cm²]. In the blend Coll-Cy7:Ch95-Cy5.5, at the ratio 1:1, the fluorescence signal corresponding to Coll-Cy7 was twice lower than the Coll-Cy7 alone showing a fluorescence value of $2.4 \times 10^9 \pm 1.5 \times 10^9$ [p/s]/[µW/cm²]. The fluorescence signal emitted by the Ch95-Cy5.5 was $2.3 \times 10^{10} \pm 2.5 \times 10^9$ [p/s]/[µW/cm²]. Moreover, fluorescence signal from Ch95-Cy5.5 in the blend Coll-Cy7:Ch95-Cy5.5 (1:1) was 20 times lower than the signal emitted by Ch95-Cy5.5 alone ($1.1 \times 10^9 \pm 9.5 \times 10^8$

[p/s]/[µW/cm²]. These results show that, for the blend Coll-Cy7:Ch95-Cy5.5 (1:1), there is a significant absorption effect of the fluorescence emitted by both fluorochromes.

Since significant variations were observed between samples of the same groups, and between samples of different groups, a normalization of the fluorescence level was necessary to obtain reliable *in vivo* results, also reducing the potential impact of the initial implant size and fluorescence heterogeneities. For all samples, the fluorescence signals at each time point were normalized by the signal obtained initially on the first day of implantation (see Equation (2)).

3.3.2. Assessment of resorption kinetics *in vivo*

The samples were implanted in mice. Figure 8A displays the evolution of fluorescence in the samples composed only by labelled collagen or labelled chitosan; it compares collagen modified by fluorochrome Cy7 (fluorescence imaging at $\lambda_{exc}/\lambda_{emi}$ 745/800 nm) and chitosan (Ch95) modified by the fluorochrome Cy5.5 (fluorescence imaging at $\lambda_{exc}/\lambda_{emi}$ 675/720 nm). Fluorescence monitoring under the skin was performed at different time points from D00 to D28. For the Coll-Cy7 sample, a decrease of the mean fluorescence signal was observed from D00 until D28. Seven days after the implantation, the fluorescence decrease was of about 30%, indicating a fast resorption of collagen. At the end of the study (D28), fluorescence was still visible with a level of about 10% of the initial fluorescence level, indicating the presence of residual Coll-Cy7 in the implanted site. This fluorescence decrease was in agreement with the histological analyses performed at D07 and D28 which showed a clear degradation of the collagen sample (see below). In the chitosan sample (Ch95:Cy5.5), a fluorescence decrease was observed at D1, possibly resulting from the degradation of the resorbable suture used to fix the samples. During all the follow-up, the fluorescence level of the Ch95-Cy5.5 sample remains close to 100% suggesting that chitosan resorption occurred very slowly in these conditions, in accordance with the histological observation (see below). These data highlight the different behaviors between collagen and chitosan, in which a sample containing only collagen presented a continuous degradation, while the samples containing only chitosan at DA ~3 % remained stable after 28 days, as a result of a much slower resorption.

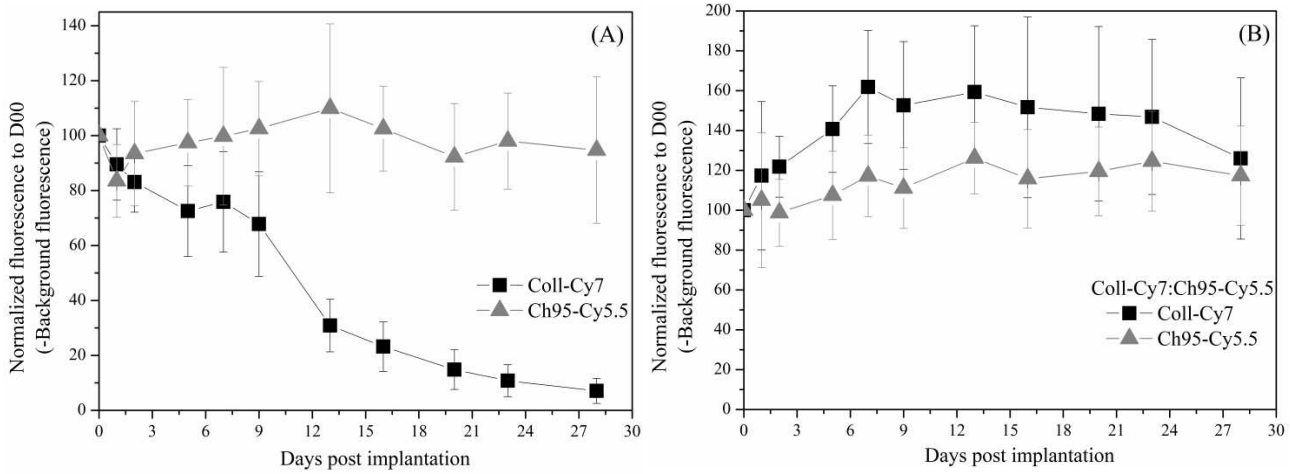

Figure 8 – Fluorescence evolution from D0 to D28 of the alone components Coll-Cy7 and Ch95-Cy5.5 (A). Fluorescence evolution of Coll-Cy7:Ch95-Cy5.5 blend, at the ratio 1:1, showing the signal corresponding to Coll-Cy7 and Ch95-Cy5.5 (B).

Coll-Cy7:Ch95-Cy5.5, at the ratio 1:1, was studied using linear spectral un-mixing facility [57] of the Perkin Elmer IVIS spectrum optical imaging system. Thus, the follow-up of each component was performed separately. However, the wavelengths of each component may not be completely separated, resulting in a follow-up that was less sensitive than with each component alone. Fluorescence kinetics of the Coll-Cy7:Ch95-Cy5.5 sample is showed in Figure 8 (B), in which the detection of each component was performed using its specific wavelength. Chitosan modified by the Cy5.5 fluorochrome in the Coll-Cy7:Ch95-Cy5.5 blend presented a similar pattern when compared with Ch95-Cy5.5 sample (Fig. 8A). Indeed, only a small variation from D00 to D28 was observed at similar fluorescence levels (near 110%). The variability is more important in these conditions than when Ch95-Cy5.5 was analyzed separately. The collagen fluorescence kinetics in the Coll-Cy7:Ch95-Cy5.5 blend presented an increase from D00 to D06 (100% to 160 %) followed by a decrease until the end of the study at D28. These samples were also studied by histological analysis to confirm the fluorescence results. Thus, the resorption kinetics of both components of the Coll:Ch blend appeared to be mainly controlled by chitosan. In the sample preparation, chitosan solution embeds the fibrils and the scaffold processing would result in hiding the collagen, coated by chitosan. Then, the degradation of collagen would be conditioned by an anterior degradation of chitosan.

As mentioned before, the concomitant Coll-Cy7 and Ch95-Cy5.5 follow-up, in the Coll-Cy7:Ch95-Cy5.5 blend, showed an initial increase in the fluorescence signal between D00 and D06 (see Figure 8B).

This behavior was not expected, and at first, we supposed that it could be explained by an optical interaction between the Cy7 (collagen) and the Cy5.5 (chitosan) fluorochromes, through: (*i*) an attenuation effect at D00 which would reduce the fluorescence level and would induce a bias in the quantification of fluorescence in the early stages of implantation. Then, rehydration and/or a partial resorption would reduce this attenuation effect, inducing an increase of the fluorescence signal; (*ii*) a self-excitation between Coll-Cy7 and Ch95-Cy5.5. The standard procedure involved an excitation at 675 nm and emission at 720 nm of Cy5.5 fluorochromes (Ch95-Cy5.5) followed shortly by an excitation at 745 nm and emission at 800 nm of Cy7 fluorochromes from Coll-Cy7. In these conditions, a side excitation of Cy7 by Cy5.5 emission would possibly impact the detection of the Coll-Cy7 leading to an overestimation of the collagen contribution. Then to avoid this artefact, the delay between Cy7 and Cy5.5 signal acquisition should be increased and/or the first fluorescence imaging should be performed on Cy7 first and then on Cy5.5. These specific experiments were performed and the results are shown in supporting material (SM-Table 2 and SM-Table 3). The main conclusion is that the fluorescence signal from one fluorochrome does not influence the emission signal from the other one. They presented almost constant emission values after the tests with the three different conditions. Then, we first tested if a difference in the fluorescence emission for both fluorochrome (Cy7 and Cy5.5) could be measured for samples analyzed in hydrated (5 min in saline solution) and dried state. Dried samples exhibited higher fluorescence intensity values in comparison with hydrated samples by 28.2 % for Cy5.5 emission and 51.4 % for Cy7 (see SM Table 2 and 3, respectively). As seen before in the PBS uptake section, when samples were hydrated, their mass increased at least 8.5 times due to the absorption of aqueous saline solution (see Figure 5). Such water uptake induces a decrease of the fluorescence signal. *In vivo*, if hydration is responsible for the evolution of fluorescence, then it can be concluded that the hydration level decreases in the implant, as a result of draining out a part of the imbibing saline solution by the surrounding tissues. This effect could induce an increase of fluorescence signal, until the sample reaches the equilibrium with the body fluids (at day 7 according to the Figure 9 (B)). Subsequently, a small decrease of the fluorescence signal could be observed, which could be more closely related to the degradation of the sample. Such effect was more apparent when analyzed by the emission of fluorochrome Cy7 bonded to collagen (decrease from 160% to 130 %, see Figure 8 (B)).

667 The same phenomenon was observed in the case of Ch95:Cy5.5 alone, which exhibits a fluorescence
668 profile comparable to that of the Coll-Cy7:Ch95-Cy5.5 blend. However, the Coll-Cy7 samples were quickly
669 degraded and only the clear decrease of fluorescence signal could be observed. The evaluation of resorption
670 kinetics deduced here is supported by the histological analyses and the results are described below.

671 **3.3.3. Histological analysis**

672 Figure 9 shows the histological analysis of samples: Coll-Cy7, Ch95-Cy5.5, Coll:Ch95 blend
673 (unlabelled, at the ratio 1:1) and Coll-Cy7:Ch95-Cy5.5 at the ratio 1:1 at D07 and D28. In Coll-Cy7 implant,
674 a yellow staining appears clearly at D07 follow-up: it corresponds to the collagen from the biomaterial,
675 which was surrounded and infiltrated by inflammatory cells from the periphery (Fig.9 A1). This
676 inflammatory reaction is typical for Coll samples in the early stages. Figure 9 B1 shows a slight
677 inflammatory reaction in the Ch95 samples, mostly due to mononuclear cells. In these samples cell
678 infiltrations were quite limited in the biomaterial that exhibited a lamellar shape after fixation at D07 follow-
679 up; this lamellar shape corresponds to the cuts of porous freeze-dried Ch95 sample described in Figure 4.
680 The unlabelled biomaterial Coll:Ch95 (ratio 1:1) induced an inflammatory reaction with mononuclear cells
681 (see Fig 9 C1) comparable with the labelled biomaterial Coll-Cy7:Ch95-Cy5.5 (ratio 1:1) (see Fig.9 D1). In
682 both cases, with unlabelled and labelled Coll:Ch95 (Fig 9 C1 and D1), the biomaterials presented a porous
683 structure partly invaded by cells at D07 follow-up.

684 At D28, the collagen sample apparently totally disappeared and the inflammatory reaction was
685 resolved as expected in this model (see Fig.9 A2). In the Ch95 samples, a slight inflammatory reaction
686 remained and the biomaterial was still present with its porous structure, as can be observed in Figure 9 B2.
687 The unlabelled Coll:Ch95 (ratio 1:1) presented a low resorption and induced an inflammatory reaction
688 comparable to that of D07 (see Fig.9 C2). Similar observations can be made for the labelled biomaterial,
689 Coll-Cy7:Ch95-Cy5.5 (ratio 1:1) (see Fig.9 D2).
690

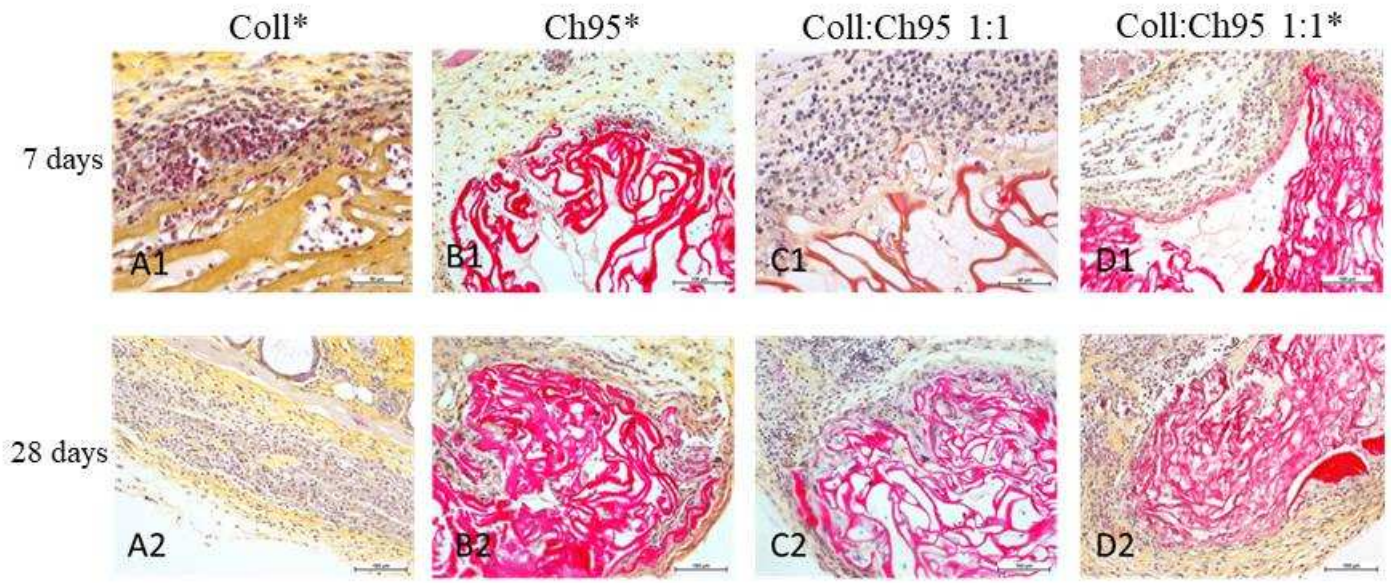

*Coll modified by Cy7; *Ch95 modified by Cy5.5;

*Coll modified by Cy7 blended with Ch95 modified by Cy5.5 at the ratio 1:1.

Figure 9 – Histological sections, showing inflammatory reaction to subcutaneously implanted biomaterials in mouse after 7 days (pictures A1 to D1) and 28 days (A2 to D2).

The histological analysis corroborated the fluorescence imaging analysis showing that collagen samples presented a high resorption at D28 whereas Ch95 and Coll:Ch95 samples presented a small resorption at the end of the study, with a limited cell infiltration and a considerable inflammatory response. In addition, labelling the polymers with the fluorochromes induced neither a modification in the inflammatory response nor a change in the resorption of the samples. These results evidence the possibility to use small quantities of fluorochromes in implantable devices without affecting the biological properties of the material.

4 - Conclusions

Scaffolds of collagen/chitosan blends for application as biomaterials were successfully prepared by the freeze-drying of mixed aqueous solution, followed by self-crosslinking via dehydrothermal treatment (DHT). Stable in aqueous solutions, these blends were characterized by several physico-chemical and structural investigation techniques: the collagen:chitosan blends formed an open structure with pore sizes compatible with cell internalization. The mechanical properties of the dry and rehydrated scaffolds are well-suited for handling and surgical procedures.

Regarding the biological evaluation, the scaffolds have been shown to be non cytotoxic *in vitro*. Their biodegradation *in vivo* could be followed by simultaneous optical fluorescence imaging of two fluorochromes. The collagen resorption could be profoundly changed by the blend formation with chitosan. In the composition range investigated, chitosan imposed the bioresorption rate of the implanted blends (mouse model).

Since collagen and chitosan are strongly interacting in the DHT-crosslinked systems, the cellular responses can not be easily predicted, since they are not a weighted average of the contribution of each component. Nevertheless these physico-chemical and biological blend property evaluations can be used to prepare a series of biomaterials with collagen:chitosan composition that will present a tunable resorption time, increasing the possibilities of applications.

Acknowledgements

The authors would like to thank the funders of this work, BPI, Grand Lyon and Region Auvergne-Rhône-Alpes (Fonds Unique Interministeriel ColoMatrix project ET2014-003). We also would like to thank the CTμ, *plateforme de microscopie multidisciplinaire*, from Université Claude Bernard Lyon 1, for the support to realise the Scanning Electron Microscope (SEM) analysis

5 - References

[1] A. Sionkowska, Current research on the blends of natural and synthetic polymers as new biomaterials: Review. Prog. Polym. Sci. 36(9) (2011) 1254-76. doi: http://dx.doi.org/10.1016/j.progpolymsci.2011.05.003.

[2] M.N. Taravel, A. Domard, Collagen and its interaction with chitosan: II. Influence of the physicochemical characteristics of collagen. Biomaterials.16(11) (1995) 865-71. doi: http://dx.doi.org/10.1016/0142-9612(95)94149-F.

[3] N. G. Oliveira, T. Sirgado, L. Reis, L.F.V. Pinto, C.L. da Silva, F.C. Ferreira, A. Rodrigues, In vitro assessment of three dimensional dense chitosan-based structures to be used as bioabsorbable implants. J. Mech. Behav. Biomed. Mater. 40 (2014) 413-25. doi: http://dx.doi.org/10.1016/j.jmbbm.2014.09.014.

[4] L. Ma, C. Gao, Z. Mao, J. Zhou, J . Shen, X. Hu, C. Han, Collagen/chitosan porous scaffolds with improved biostability for skin tissue engineering. Biomaterials. 24(26) (2003) 4833-41. doi: http://dx.doi.org/10.1016/S0142-9612(03)00374-0.

[5] S.Z. Rogovina, G.A.Vikhoreva, Polysaccharide-based polymer blends: Methods of their production. Glycoconjugate J. 23(7) (2006) 611-18. doi: 10.1007/s10719-006-8768-7.

[6] H.-F. Ko, C. Sfeir, P.N. Kumta, Novel synthesis strategies for natural polymer and composite biomaterials as potential scaffolds for tissue engineering. Philos. Trans A, Math. Phys. Eng Sci. 368(1917) (2010) 1981-97. doi: 10.1098/rsta.2010.0009. PubMed PMID: PMC2944391.

[7] I.V. Yannas, D.S. Tzeranis, B.A. Harley, P.T.C. So, Biologically active collagen-based scaffolds: advances in processing and characterization. Philos. Trans A, Math. Phys. Eng Sci. 368(1917) (2010) 2123-39. doi: 10.1098/rsta.2010.0015

[8] R.K. Perumal, S. Perumal, T. Ramar, A. Gopinath, S.K. Ramadass, B. Madhan, S. Sirvasubramanian. Collagen-fucoidan blend film with the potential to induce fibroblast proliferation for regenerative applications. Int. J. Biol. Macromol. 106 (2018) 1032-40. doi: https://doi.org/10.1016/j.ijbiomac.2017.08.111.

[9] H. Kenar, C.Y. Ozdogan, C. Dumlu, E. Doger, G.T. Kose, V. Hasirci, Microfibrous scaffolds from poly(l-lactide-co-ε-caprolactone) blended with xeno-free collagen/hyaluronic acid for improvement of vascularization in tissue engineering applications. Mater. Sci. Eng. C. 97 (2019) 31-44. doi: https://doi.org/10.1016/j.msec.2018.12.011

[10] D.E. Birk, P. Bruckner, Collagen Suprastructures. In: J. Brinckmann, H. Notbohm, P.K. Müller, editors. Collagen: Primer in Structure, Processing and Assembly. Berlin, Heidelberg: Springer Berlin Heidelberg; 2005. p. 185-205.

[11] R. Zine, M. Sinha, Nanofibrous poly(3-hydroxybutyrate-co-3-hydroxyvalerate)/collagen/graphene oxide scaffolds for wound coverage. Mater. Sci. Eng. C. 80(Supplement C) (2017) 129-34. doi: https://doi.org/10.1016/j.msec.2017.05.138.

[12] X. He, X. Fan, W. Feng, Y. Chen, T. Guo, F. Wang, J. Liu, K. Tang,. Incorporation of microfibrillated cellulose into collagen-hydroxyapatite scaffold for bone tissue engineering. Int. J. Biol. Macromol. 115 (2018) 385-92. doi: https://doi.org/10.1016/j.ijbiomac.2018.04.085

[13] G.A.F. Roberts. Chitin Chemistry. The Macmillan Press Ltd., Hong Kong, 1992.

[14] N. Boucard, L. David, C. Rochas, A. Montembault, C. Viton, A. Domard, Polyelectrolyte Microstructure in Chitosan Aqueous and Alcohol Solutions. Biomacromolecules. 8(4) (2007) 1209-17. doi: https://doi.org/10.1021/bm060911m.

[15] J. Becerra, G. Sudre, I. Royaud, R. Montserret, B. Verrier, C. Rochas, T. Delair, L. David, Tuning the Hydrophilic/Hydrophobic Balance to Control the Structure of Chitosan Films and Their Protein Release Behavior. AAPS PharmSciTech. 18(4) (2017) 1070-83. doi: 10.1208/s12249-016-0678-9.

[16] K. Tomihata, Y. Ikada In vitro and in vivo degradation of films of chitin and its deacetylated derivatives. Biomaterials. 18(7) (1997) 567-75. doi: https://doi.org/10.1016/S0142-9612(96)00167-6.

[17] F. Croisier, C. Jérôme, Chitosan-based biomaterials for tissue engineering. Eur. Polym. J. 49(4) (2013) 780-92. doi: https://doi.org/10.1016/j.eurpolymj.2012.12.009.

[18] M. Rinaudo. Chitin and chitosan: Properties and applications. Prog. Polym. Sci. 31(7) (2006) 603-32. doi: https://doi.org/10.1016/j.progpolymsci.2006.06.001.

[19] T. Barroso, R. Viveiros, T. Casimiro, A. Aguiar-Ricardo, Development of dual-responsive chitosan–collagen scaffolds for pulsatile release of bioactive molecules. J. Supercrit. Fluid. 94 (2014) 102-12. doi: http://dx.doi.org/10.1016/j.supflu.2014.07.005.

[20] F. Wang, M. Wang, Z. She, K. Fan, C. Xu, B. Chu, C. Chen, S. Shi, R. Tan, Collagen/chitosan based two-compartment and bi-functional dermal scaffolds for skin regeneration. Mater. Sci. Eng. C. 52 (2015) 155-62. doi: http://dx.doi.org/10.1016/j.msec.2015.03.013.

[21] J. Lewandowska-Łańcucka, S. Fiejdasz, A. Łatkiewicz, M. Nowakowska, Ł. Rodzik, Novel hybrid materials for preparation of bone tissue engineering scaffolds. J. Mater. Sci. Mater. Med. 26(9) (2015) 231-46. doi: 10.1007/s10856-015-5564-6.

[22] L.A. Reis, L.L.Y. Chiu, Y. Liang, K. Hyunh, A. Momen, M. Radisic, A peptide-modified chitosan–collagen hydrogel for cardiac cell culture and delivery. Acta Biomater. 8(3) (2012) 1022-36. doi: https://doi.org/10.1016/j.actbio.2011.11.030.

[23] X. Wang, L. Sang, D. Luo, X. Li, From collagen–chitosan blends to three-dimensional scaffolds: The influences of chitosan on collagen nanofibrillar structure and mechanical property. Colloids Surf. B Biointerfaces. 82(1) (2011) 233-40. doi: http://dx.doi.org/10.1016/j.colsurfb.2010.08.047.

[24] A. Martínez, M.D. Blanco, N. Davidenko, R.E. Cameron, Tailoring chitosan/collagen scaffolds for tissue engineering: Effect of composition and different crosslinking agents on scaffold properties. Carbohyd. Polym. 132(Supplement C) (2015) 606-19. doi: https://doi.org/10.1016/j.carbpol.2015.06.084.

[25] T. Yan, F. Cheng, X. Wei, Y. Huang, J. He, Biodegradable collagen sponge reinforced with chitosan/calcium pyrophosphate nanoflowers for rapid hemostasis. Carbohyd. Polym. 170(Supplement C) (2017) 271-80. doi: https://doi.org/10.1016/j.carbpol.2017.04.080.

[26] Y. Zhu, T. Liu, K. Song, B. Jiang, X. Ma, Z. Cui, Collagen–chitosan polymer as a scaffold for the proliferation of human adipose tissue-derived stem cells. J. Mater. Sci. Mater. Med. 20(3) (2009) 799-808. doi: 10.1007/s10856-008-3636-6.

[27] T.J. Wess, J.P. Orgel, Changes in collagen structure: drying, dehydrothermal treatment and relation to long term deterioration. Thermochim. Acta. 365(1–2) (2000) 119-28. doi: http://dx.doi.org/10.1016/S0040-6031(00)00619-5.

[28] I.V. Yannas, A.V. Tobolsky, Cross-linking of Gelatine by Dehydration. Nature. 215(5100) (1967) 509-10. doi:10.1038/215509b0

[29] M.G. Haugh, M.J. Jaasma, F.J. O'Brien, The effect of dehydrothermal treatment on the mechanical and structural properties of collagen-GAG scaffolds. J. Biomed. Mater. Res. A. 89A(2) (2009) 363-9. doi: 10.1002/jbm.a.31955.

[30] P. Jithendra, A.M. Rajam, T. Kalaivani, A.B. Mandal, C. Rose, Preparation and Characterization of Aloe Vera Blended Collagen-Chitosan Composite Scaffold for Tissue Engineering Applications. ACS Appl. Mater. Inter. 5(15) (2013) 7291-8. doi: 10.1021/am401637c.

[31] S. Yunoki, N. Nagai, T. Suzuki, M. Munekata, Novel biomaterial from reinforced salmon collagen gel prepared by fibril formation and cross-linking. J. Biosci. Bioeng. 98(1) (2004) 40-7. doi: https://doi.org/10.1016/S1389-1723(04)70240-6.

[32] T. Ahmad, H. Bae H, Y. Iqbal, I. Rhee, S. Hong, Y. Chang, J. Lee, D. Sohn, Chitosan-coated nickel-ferrite nanoparticles as contrast agents in magnetic resonance imaging. J. Magn. Magn. Mater. 381(Supplement C) (2015) 151-7. doi: https://doi.org/10.1016/j.jmmm.2014.12.077.

[33] K. Lei, Y. Chen, J. Wang, X. Peng, L. Yu, J. Ding, Non-invasive monitoring of in vivo degradation of a radiopaque thermoreversible hydrogel and its efficacy in preventing post-operative adhesions. Acta Biomater. 55(Supplement C) (2017) 396-409. doi: https://doi.org/10.1016/j.actbio.2017.03.042.

[34] N. Artzi, N. Oliva, C. Puron, S. Shitreet, S. Artzi, A. bon Ramos, A. Grootuis, G. Sahagian, E.R. Edelman, In vivo and in vitro tracking of erosion in biodegradable materials using non-invasive fluorescence imaging. Nat Mater. 10 (2011) 704-709. doi: 10.1038/NMAT3095

[35] R.I. Dmitriev, S.M. Borisov, H. Düssmann, S. Sun, B.J. Müller, J. Prehn, V.P. Baklaushev, I. Klimant, D.B. Papkvsky, Versatile Conjugated Polymer Nanoparticles for High-Resolution O2 Imaging in Cells and 3D Tissue Models. ACS Nano. 9(5) (2015) 5275-88. doi: 10.1021/acsnano.5b00771.

[36] N. Rescignano, L. Tarpani, A. Romani, I. Bicchi, S. Mattioli, C. Emiliani, L. Torre, J.M. Kenny, S. Martino, L. Latterini, I. Armentano, In-vitro degradation of PLGA nanoparticles in aqueous medium and in stem cell cultures by monitoring the cargo fluorescence spectrum. Polym. Degrad. Stabil. 134(Supplement C): (2016) 296-304. doi: https://doi.org/10.1016/j.polymdegradstab.2016.10.017.

[37] Y. Zhang, F. Rossi, S. Papa, M.B. Violatto, P. Bigini, M. Sorbona, F. Redaelli, P. Veglianese, J. Hilborn, D. Ossipov, Non-invasive in vitro and in vivo monitoring of degradation of fluorescently labeled hyaluronan hydrogels for tissue engineering applications. Acta Biomater. 30 (2016) 188-98. doi: https://doi.org/10.1016/j.actbio.2015.11.053.

[38] C. Cunha-Reis, A.J. El Haj, X. Yang, Y. Yang, Fluorescent labeling of chitosan for use in non-invasive monitoring of degradation in tissue engineering. J. Tissue Eng. Regen. M. 7(1) (2013) 39-50. doi: 10.1002/term.494.

[39] X. Dong, C. Wei, L. Lu, T. Liu, F. Lv, Fluorescent nanogel based on four-arm PEG–PCL copolymer with porphyrin core for bioimaging. Mater. Sci. Eng. C. 61 (2016) 214-9. doi: https://doi.org/10.1016/j.msec.2015.12.037.

[40] F. Lv, L. Mao, T. Liu, Thermosensitive porphyrin-incorporated hydrogel with four-arm PEG–PCL copolymer: Preparation, characterization and fluorescence imaging in vivo. Mater. Sci. Eng. C. 43(Supplement C) (2014) 221-30. doi: https://doi.org/10.1016/j.msec.2014.07.019.

[41] A. Hirai, H. Odani, A. Nakajima, Determination of degree of deacetylation of chitosan by 1H NMR spectroscopy. Polymer Bulletin. 26(1) (1991) 87-94. doi: 10.1007/BF00299352.

[42] C. Schatz, C. Viton, T. Delair, C. Pichot, A. Domard, Typical Physicochemical Behaviors of Chitosan in Aqueous Solution. Biomacromolecules. 4(3) (2003) 641-8. doi: 10.1021/bm025724c.

[43] E. Borenfreund, J.A. Puerner, Toxicity determined in vitro by morphological alterations and neutral red absorption. Toxicol. Lett. 24(2) (1985) 119-24. doi: https://doi.org/10.1016/0378-4274(85)90046-3.

[44] T. Mosmann, Rapid Colorimetric Assay For Cellular Growth And Survival - Application To Proliferation And Cyto-Toxicity Assays. J Immol Methods 65(1-2) (1984) 55-63.

[45] M.M. Horn, V.C.A. Martins, A.M. de Guzzi Plepis, Interaction of anionic collagen with chitosan: Effect on thermal and morphological characteristics. Carbohyd. Polym. 77(2) (2009) 239-43. doi: https://doi.org/10.1016/j.carbpol.2008.12.039.

[46] Y.S. Nam, W.H. Park, D. Ihm, S.M. Hudson, Effect of the degree of deacetylation on the thermal decomposition of chitin and chitosan nanofibers. Carbohyd. Polym. 80(1) (2010) 291-5. doi: https://doi.org/10.1016/j.carbpol.2009.11.030.

[47] D. de Britto, S.P. Campana-Filho, Kinetics of the thermal degradation of chitosan. Thermochim. Acta. 465(1) (2007) 73-82. doi: https://doi.org/10.1016/j.tca.2007.09.008.

[48] M.L. Duarte, M.C. Ferreira, M.R. Marvão, J. Rocha, An optimised method to determine the degree of acetylation of chitin and chitosan by FTIR spectroscopy. Int. J. Biol. Macromol. 31(1) (2002) 1-8. doi: https://doi.org/10.1016/S0141-8130(02)00039-9.

[49] A. Zając, J. Hanuza, M. Wandas, L. Dymińska, Determination of N-acetylation degree in chitosan using Raman spectroscopy. Spectrochim. Acta A Mol. Biomol. Spectrosc. 134 (2015) 114-20. doi: https://doi.org/10.1016/j.saa.2014.06.071.

[50] A.M.D. Guzzi Plepis, G. Goissis, D.K. Das-Gupta, Dielectric and pyroelectric characterization of anionic and native collagen. Polym. Eng. Sci. 36(24) (1996) 2932-8. doi: 10.1002/pen.10694.

[51] M. Jackson, L.-Pi Choo , P.H. Watson, W.C. Halliday, H.H. Mantsch, Beware of connective tissue proteins: Assignment and implications of collagen absorptions in infrared spectra of human tissues. Biochim. Biophys. Acta Mol. Basis Dis. 1270(1) (1995) 1-6. doi: https://doi.org/10.1016/0925-4439(94)00056-V.

[52] J.H. Muyonga, C.G.B. Cole, K.G. Duodu, Characterisation of acid soluble collagen from skins of young and adult Nile perch (Lates niloticus). Food Chem. 85(1) (2004) 81-9. doi: https://doi.org/10.1016/j.foodchem.2003.06.006.

[53] P.L. Gordon, C. Huang, R.C. Lord, I.V. Yannas, The Far-Infrared Spectrum of Collagen. Macromolecules. 7(6) (1974) 954-6. doi: 10.1021/ma60042a052.

[54] M. Madaghiele, E. Calò, L. Salvatore, V. Bonfrate, D. Pedone, M. Frigione, A. Sannino, Assessment of collagen crosslinking and denaturation for the design of regenerative scaffolds. J. Biomed. Mater. Res. A. 104(1) (2016) 186-94. doi: 10.1002/jbm.a.35554.

[55] H. Cao, S.-Y. Xu, Purification and characterization of type II collagen from chick sternal cartilage. Food Chem. 108(2) (2008) 439-45. doi: https://doi.org/10.1016/j.foodchem.2007.09.022.

[56] N. Dagalakis, J. Flink, P. Stasikelis, J.F. Burke, I.V. Yannas, Design of an artificial skin. Part III. Control of pore structure. J. Biomed. Mater. Res. 14(4) (1980) 511-28. doi: 10.1002/jbm.820140417.

[57] T. Zimmermann, J. Marrison, J. Hogg, P. O'Toole, Clearing up the signal: imaging and linear unmixing in fluorescence microscopy. In: W. PS, editor. Confocal microscopy: methods and protocols, methods in molecular biology. 1075. New York Springer Science and Business Media 2014.